LAMINAR BURNING SPEED MEASURMENTS OF METHANE /AIR/CARBON DIOXIDE MIXTURES

A Thesis Presented

By

Moaz Omar Allehaibi

to

The Department of Mechanical and Industrial Engineering

In partial fulfillment of the requirements

for the degree of

Master of Science

in the field of

Mechanical Engineering

Northeastern University

Boston, Massachusetts

May 2017

ABSTRACT

Land Fill Gas (LFG) and Biogas are mixtures of methane (CH_4) / carbon dioxide (CO_2) that can be used as energy source in combustors. The presence of CO_2 reduces the energy content per unit mass of these gases and negatively impacts the combustion stability. Laminar burning speeds of simulated LFG have been measured in this study.

The experiments were conducted in a constant volume cylindrical chamber with the aid of a Z-shaped Schlieren/shadowgraph system. Pressure rise data during the flame propagation were recorded through pressure transducer on the cylindrical chamber wall and were the main input into the thermodynamic model used to measure the laminar burning speed. A high-speed CMOS camera capable of taking pictures up to 40,000 frames per second was used to determine the cellularity of the flame.

Pictures of the CH_4/air/ CO_2 flames for different equivalence ratios and carbon dioxide percentages were taken. As the CO_2 mole fraction increased the flame is less prone to become cellular. Fuel rich mixtures are less likely to become cellular than fuel lean mixtures.

Experiments of CH_4/air/ CO_2 mixtures have been conducted to simulate LFG/Biogas and laminar burning speeds were measured. The testing sets included three CO_2 mole fractions Xco_2= 0%, 20%, and 30% at two initial pressures P_i= 1 atm and 2 atm. Moreover, the set covered three initial temperatures T_i =298 K, 330 K, and 360 K and three fuel air equivalence ratios of ϕ = 0.8,1.0, and 1.2.

The effect of CO_2 on laminar burning speed was determined. As the CO_2 mole fraction increased from 0 to 30% the laminar burning speeds decreased. Moreover, data show that the laminar burning speed of CH_4/air/ CO_2 mixtures reduces with increasing pressure and increases with increasing temperature. The results show, the lowest laminar burning speed was measured at Pi = 2 atm, Ti = 298 K, ϕ = 0.8, and Xco_2= 30%.

ACKNOWKEDGMENT

I would like to express my appreciation to Professor Hameed Metghalchi for his support and guidance during the learning journey at the combustion laboratory in Northeastern University. Moreover, I would like to extend my appreciation to the laboratory technician Kevin McCue and to my teammates Kevin Vien, Ziyu Wang, Guangying Yu, and Mohammed Alswat for their corporation and effort during the research process.

My parents provided the love and the support that is crucial for me to keep pursuing knowledge and dream big. My wife, Nada Alsaeidi, kept encouraging me to keep a good balance between knowledge and my social life. My sweetest daughter, Lana, kept the smile on my face with her jokes.

To my future me, never stop pursuing knowledge. Be wiser. Be smarter. Be happier.

TABLE OF CONTENTS

List of Figures

List of Tables

1. Introduction

"In an ideal world, the design engineer would have available a complete set of measured values of all relevant properties. This is seldom the reality, however, and designers must often resort to (often crude) approximations of physical properties that are of questionable validity" [1].

The measurement of all relevant properties under all conditions is impossible [2]. Material properties are generally divided into two main categories physical and chemical properties. When designing a new process combination of these two properties are essential. The distinction between physical and chemical properties is not absolute but generally the chemical properties are related to the nature and magnitude of the intermolecular interactions. For example, detailed causes of the molecules collisions, complexing, and reacting. On the other hand, physical properties address the consequence of the chemical properties. The boiling temperature is a physical property that is the consequence of polarity, acidity or basicity (the latter are chemical properties) [2]. A physical can be measured or observed without changing the composition of the sample.

1.1. Background

Laminar burning speed (LBS) "is defined as the speed of the combustion wave normal to itself and relative to the unburned gas" [3]. It is a property that combines physical and chemical properties as well. The term physiochemical property is used in the literature to describe LBS [1]. There are many advantages of calculating the LBS, as Parsinejad [1] explains it in his thesis:

"The mass burning rates and burning speeds of homogenous fuel/oxygen/diluent gas mixtures are important both for developing and testing fluid dynamic and chemical kinetic models of hydrocarbon oxidation and for a wide range of direct practical applications in the fields of engines, burners, explosions, and chemical processors" [1]. There are many parameters that affect the LBS such as Temperature, Pressure, equivalence ratio, diluent, and fuel type.

1.2. Different Methods of Measuring Laminar Burning Speed (LBS)

There are two main approaches in measuring the LBS. Both are related to the position of the coordinates. If the coordinate system is fixed, then the flame will propagate away, hence the name propagating flame. If, on the other hand, the coordinate system is placed on top of the flame and moves with it the flame, it is said to be stationary. Flat flame burners, Bunsen burners, and stagnation burners all use stationary flame approach to measure LBS, whereas expanding spherical flames use the propagation approach.

In the stationary flat flame a jet of fuel enters the flame and for the stabilized flame the speed of the jet is equal to the burning speed of the flame. Many vertical channels are used in these experiments to make sure the flame is flat. The lack of consistence results and the difficulty of measuring LBS above 20 cm/s are the two-main limitation of this approach [4]. The mass balance for flat flame burner is given by equation (1).

$$\rho_u S_L A \equiv \rho_u v_u A = \rho_b v_b A \tag{1}$$

If we consider hydrocarbon-air flame at 1 atm. the density ratio be comes $\frac{\rho_u}{\rho_b} \approx 7$ from this, we notice that $\frac{1}{7} v_b \approx S_L$.

In the propagating approach, the flame starts from one point and moves away from it. Pressure is constant for a period of time then the pressure increases. Using the constant pressure data, burning speed can be measured with need of stain correction for initial condition. As flame propagate pressure inside the vessel is increased. Burning speed can be measured as pressure is increased and LBS can be calculated for many states during one experiment.

1.3. Purpose of Research

The addition of CO_2 to CH_4/air will be investigated experimentally to simulate the Land Fill Gas (LFG) content that is deliverable from municipal waste decommission. LFG can be used in internal combustion engines but the large quantities of CO_2 effects the burning speed and stability of these engines [5]. Hinton and Stone [6] measured laminar burning speed of CH_4/air/CO_2 mixtures and developed a correlation that is valid between 380 K $\leq T_i \leq$ 520 K, and 1 bar $\leq$ Pi $\leq$ 8 bar [6]. This thesis will measure burning speed for larger range of T_i , P_i , ϕ , and Xco_2 mentioned in Table 1. In this study 54 initial conditions were chosen and experiments were made. Laminar burning speeds were measured along these 54 isotopes. Table 1 shows the test condition.

Table 1: Test conditions

Set 1: T_i = 298 K, P_i = 1 atm. Set 2: T_i = 298 K, P_i = 2 atm. Set 3: T_i = 330 K, P_i = 1 atm. Set 4: T_i = 330 K, P_i = 2 atm. Set 5: T_i = 360 K, P_i = 1 atm. Set 6: T_i = 360 K, P_i = 2 atm.		ϕ		
		0.8	1	1.2
Xco_2%	0	x	x	x
	20	x	x	x
	30	x	x	x

2. Laboratory Facilities

Northeastern combustion laboratory was established in 1995 by Ulinski, Elia, and Moore [1]. In 2005, Parsinejad [1] built liquid fuel injection system, which made it possible to vaporize the liquid fuel and inject it into either the cylindrical or spherical vessel [1]. In summer of 2016, leaks were reported so valves and tubes have been replaced by new ones.

2.1. Supply Systems

2.1.1. Gas Manifold

The Gas manifold system consists of five gas cylinders and two vacuum pumps. The gas cylinders include methane, air, nitrogen, hydrogen, and carbon monoxide. Since there are five inlet valves, the gas manifold can accommodate up to five different gases at a time. It's also possible to increase the gaseous input to more than five by simply connecting the valve connection to any number of desirable gas cylinders after each filling. The two vacuum pumps are identical of rotary vane type. The pumps are connected to ½ HP motor by belts. These pumps are best suited for corrosive gases [7]. The manifold layout is shown in Figures 2 and 3. The pump suction line was upgraded from ¼ inch SS tube to ¾ inch hose, which reduced the vacuuming time.

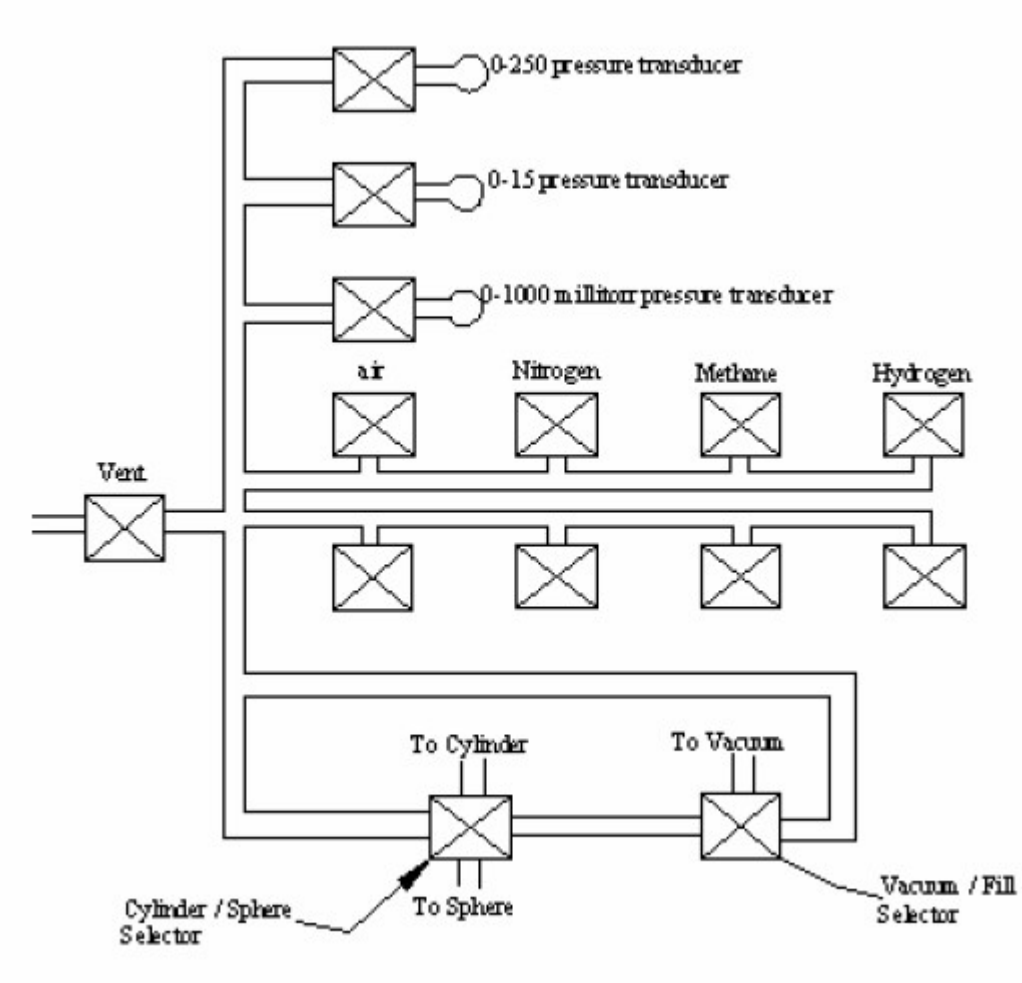

Figure 1: Manifold layout

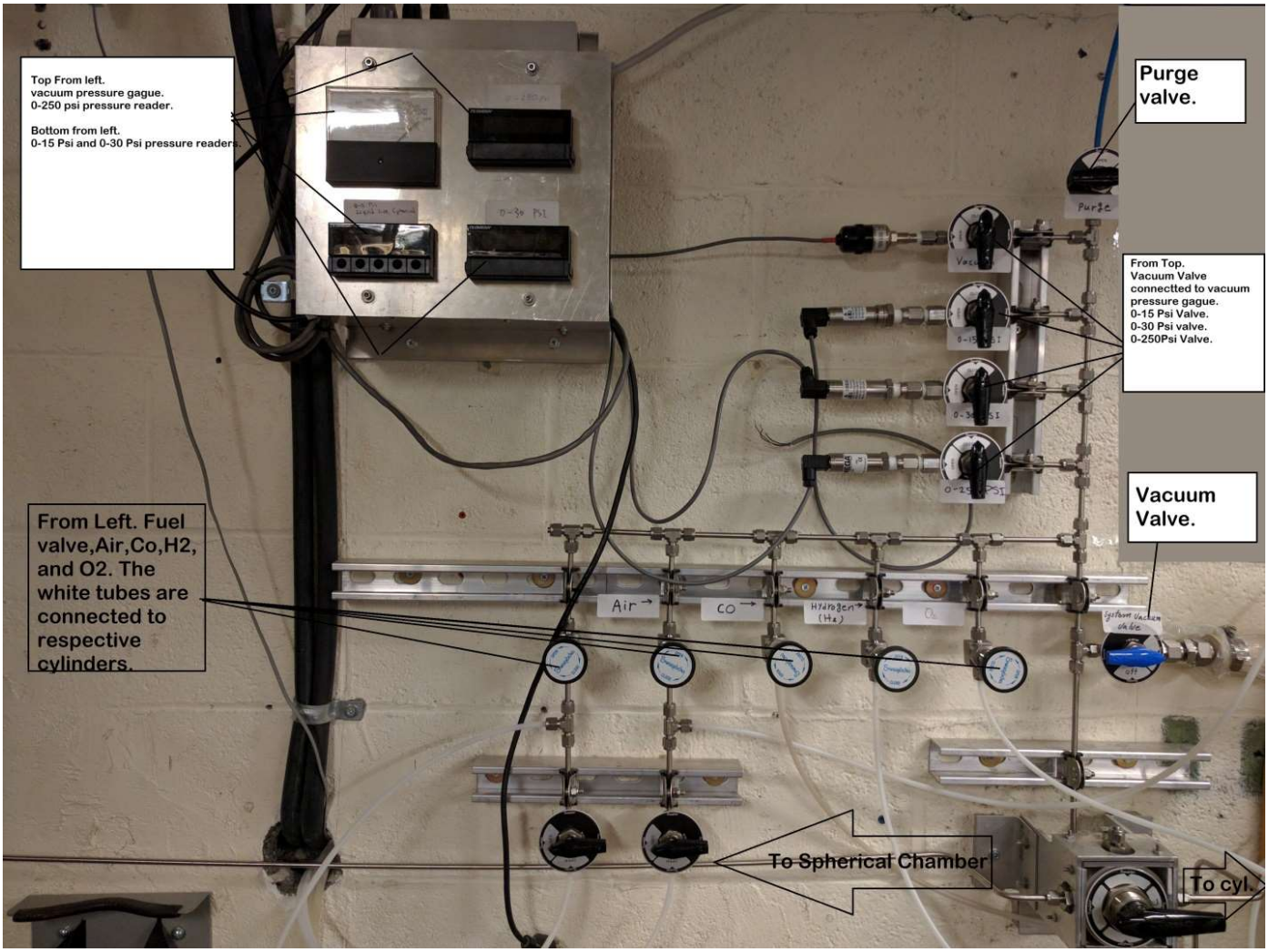

Figure 2: Gas Manifold

2.1.2. Liquid Injection

There are two separate liquid injection systems one for each combustion chamber. Each system consists of a small tank with capacity of 115 cm^3 [8]. The fuel is manually poured into and a heated section to vaporize the liquid fuel. The tubes are of 1/8-inch diameter. The fuel after vaporization is driven naturally to either the cylindrical or spherical chamber. The design of this system enabled Parisnejad [1] to calculate the laminar burning speed of JP-10 and JP-8.

2.2. Combustion Chambers

There are two types of combustion chambers in Northeastern university laboratory, cylindrical and spherical chambers. Both have the same gas manifold but separate liquid injection systems. The cylindrical chamber has glass windows on both sides, which allows to visually inspect the flame propagation and inspect cellularity as well. The spherical chamber on the other hand has ionization probes that would check the flame arrival time and gives signal to ensure that the flame touches the wall at the same time, this helps the experimenter know if the flame is buoyant or not.

2.2.1. Cylindrical Chamber

The cylindrical chamber shell and flanges are made of 316 SS, which has an inner diameter of 13.5 cm and 13 cm in length [1].The flanges hold the glass window to the shell by four bolts. The windows are made of 3.5 cm Pyrex glass that with stand pressures up to 50 atm. Figures 4 and 5 give very detailed dimensional drawings that were developed by Parisnejad [1].

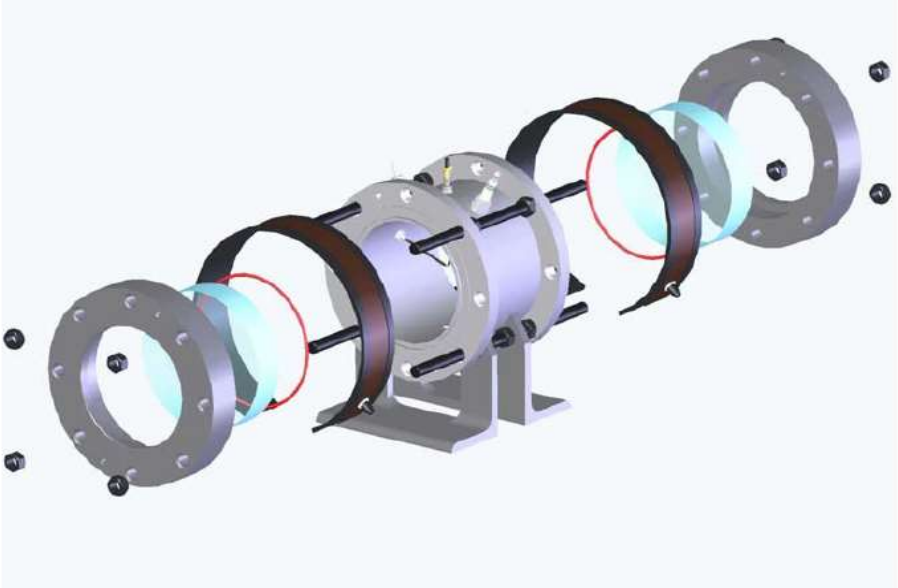

Figure 3: Cylindrical combustion vessel with exploded view

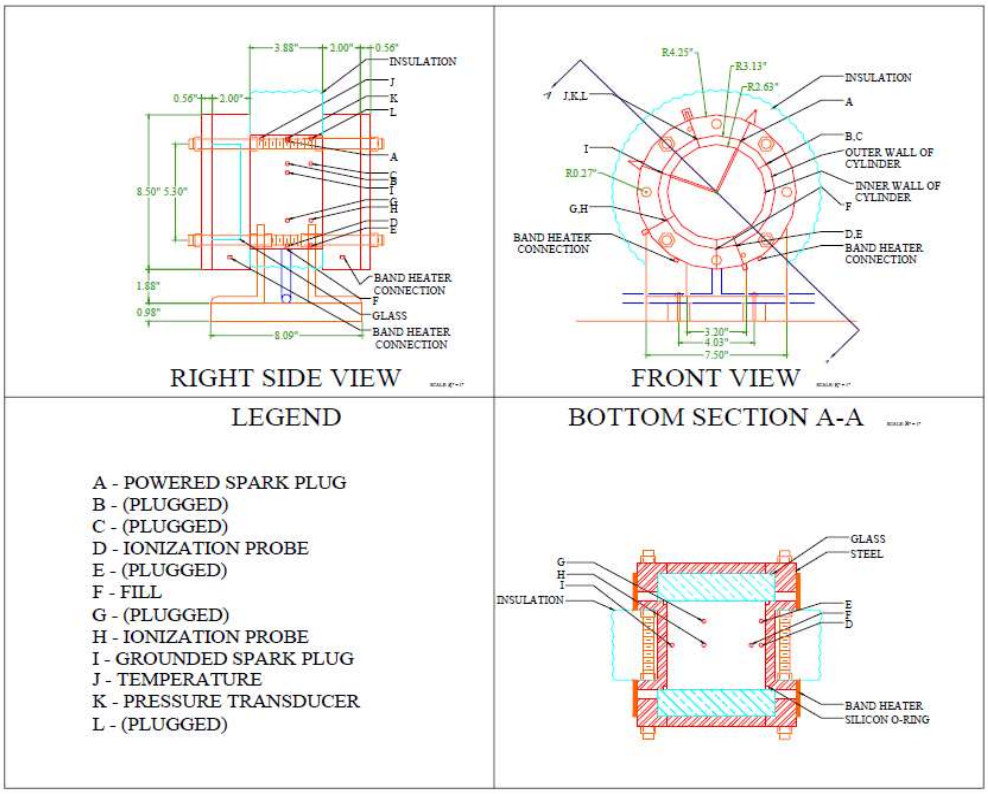

Figure 4: Schematic diagram of the cylindrical vessel

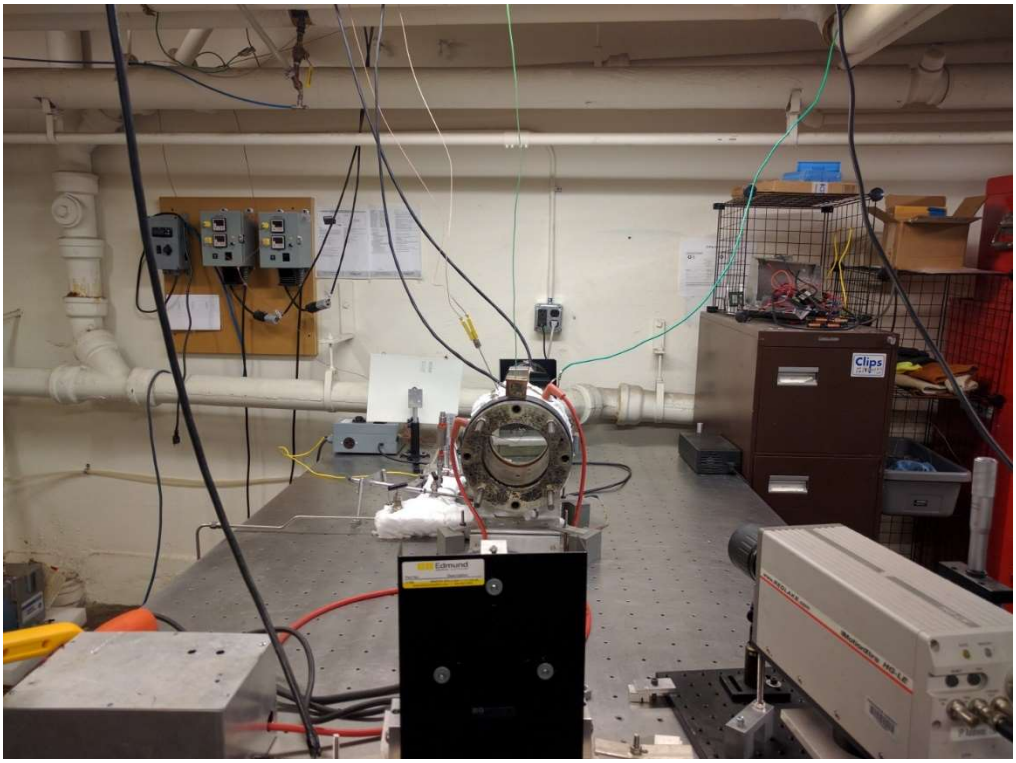

Figure 5: Cylindrical Chamber Front View

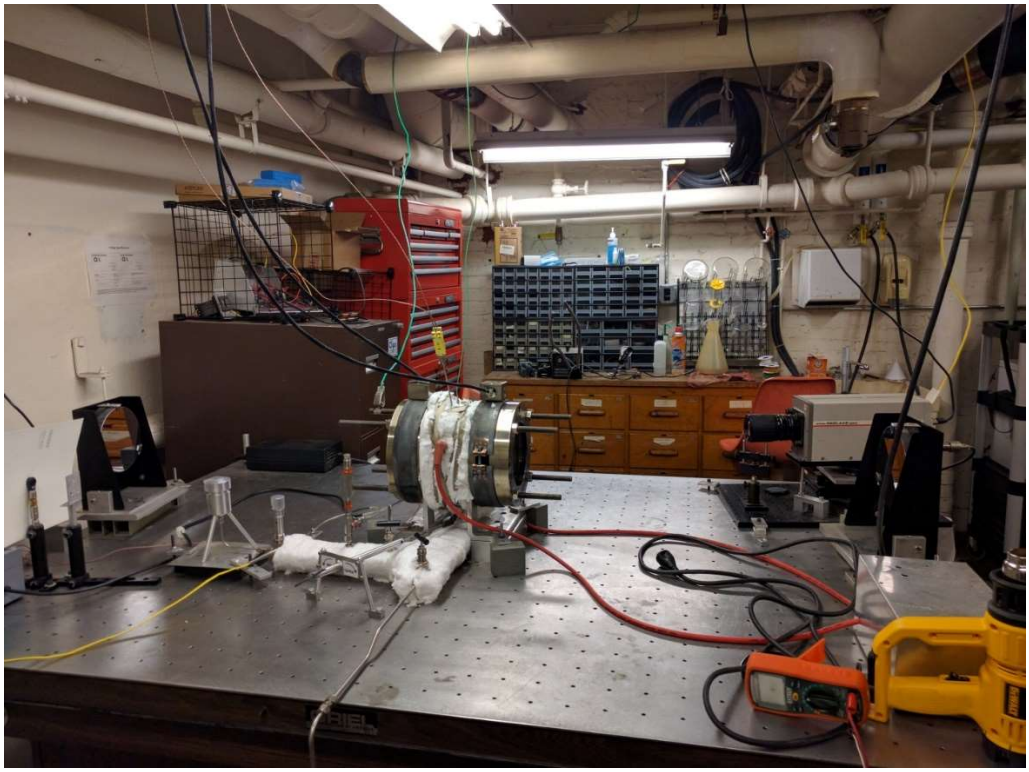

Figure 6: Cylindrical Chamber Side view

2.2.2. Spherical Chamber

Unlike the cylindrical chamber the spherical chamber is made of 4140 steel that can withstand pressures of 425 atm when using 8 bolts for tightening [9]. Although Metghalchi [10] used a smaller thickness for his experiment back in 1980, the material was 4150 FM annealed alloy steel raising pressure limit to 680 atm. Figures 6 and 7 provides a detailed schematic which were developed by Parisnejad [1].

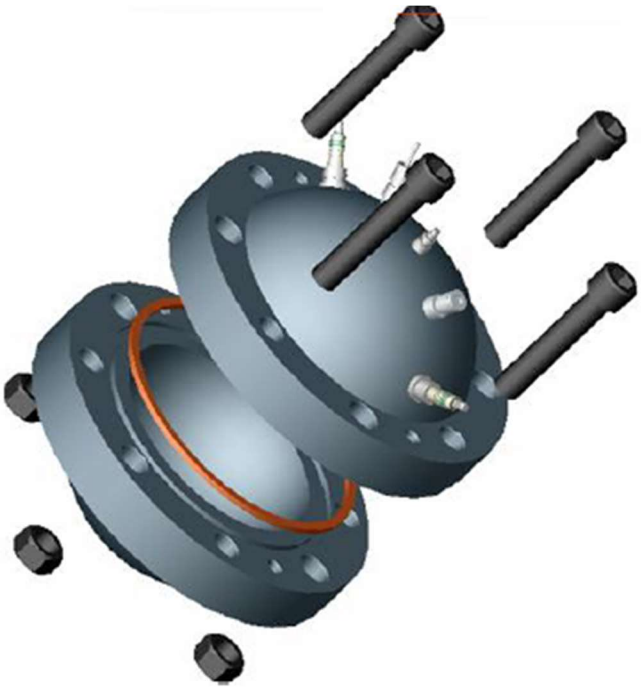

Figure 7: Spherical vessel with exploded view

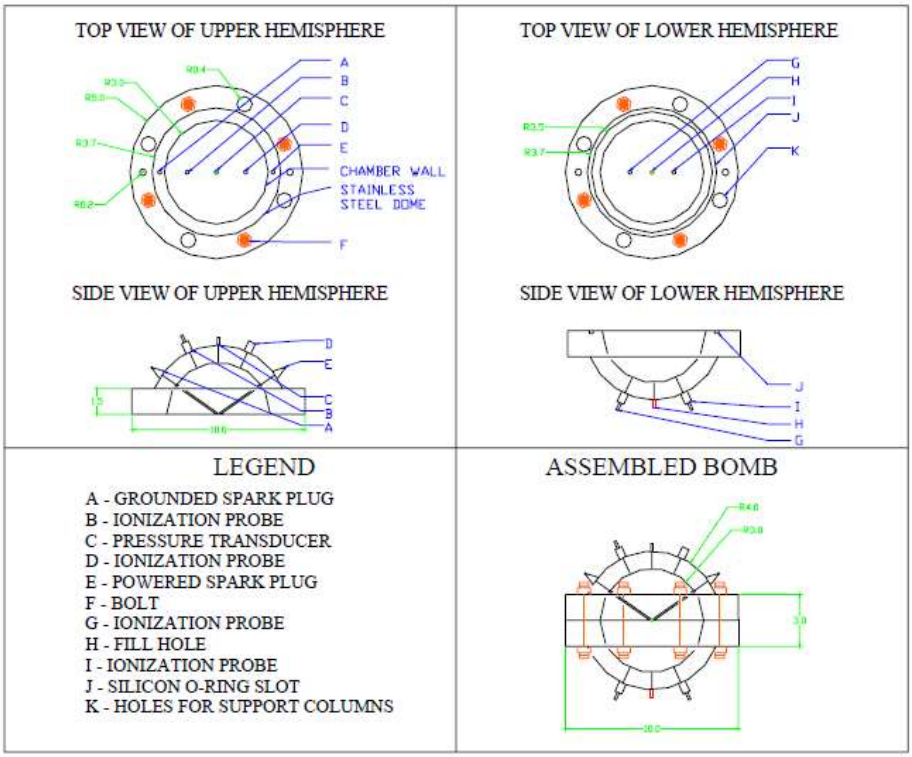

Figure 8: Schematic diagram of spherical vessel

2.3. Data Acquisition System

The data acquisition system can be divided into three major categories pressure transducer on the vessel, Kistler pressure single amplifier, and analog to digital converter box. These three divisions are seen in figure 10. The pressure transducer enables the experimenter to fill the vessel to the desired partial pressures by reading from the strain gauges shown in Figure 3. Kistler amplifier converts the signals from 4-20 mA to 10mV/psia which then processed via 16-bit converter in the analog to digital converter [3]. The analog to digital box reads the voltage difference when the flame reaches the probes. Moreover, it begins recording the pressure time signals that is the main input to the code for calculating the laminar burning speed [3].

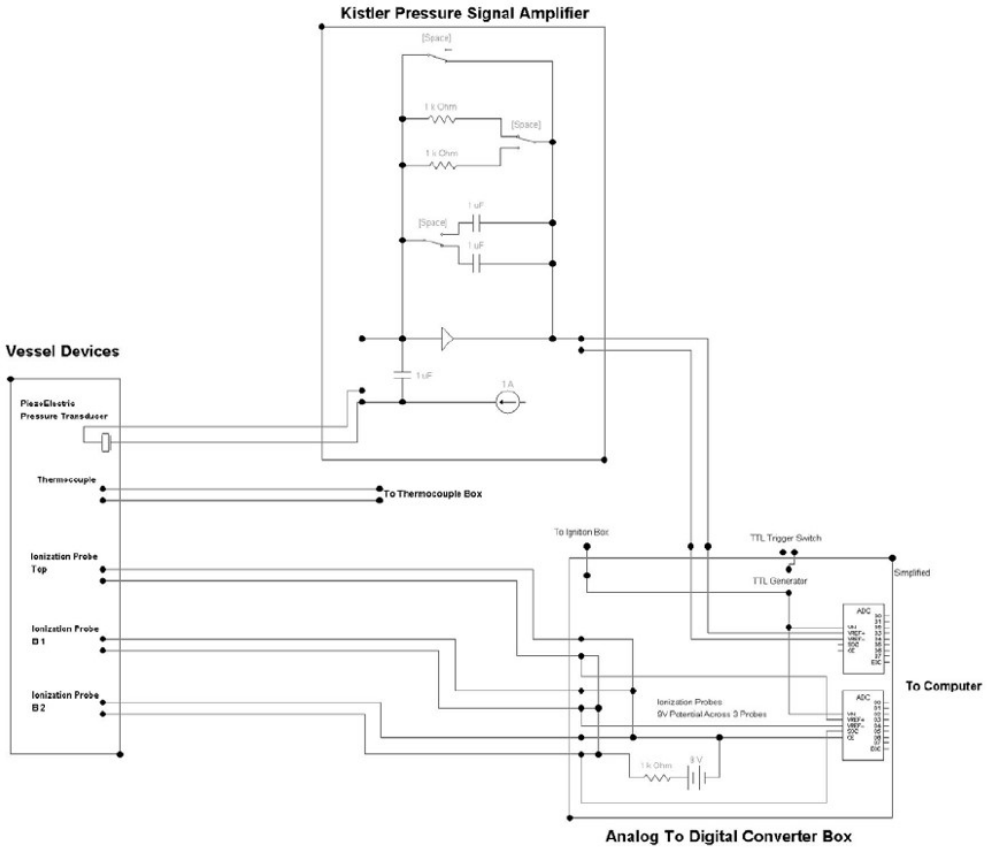

Figure 9: Data Acquisition system [3]

2.4. Flame Photography System (Schlieren System).

Although the spherical combustion chamber can be equipped with Schlieren system as seen in Mannaa [11], the laboratory in Northeastern University only has that system installed on the cylindrical chamber. Unlike the spherical chamber where the ionization probes are used to determine the flame arrival time, the flame can be observed and the arrival time can be read from pictures in the cylindrical chamber. This section aims to briefly describe the Schlieren system.

The six components shown in Figure 10 in the Schlieren system are light source, condenser lens, pinhole, two parabolic mirrors, and high speed camera. The light source is 10-Watt Halogen bulb connected to 185 mm black tube. The condenser of Thorlab Ac127-075-A-ML type that is placed 75 mm from pinhole and has the capability to focus the light to 3.6 um single spot [12]. The pinhole is 0.3 mm in diameter, which has the capability of sharpening the image. Figure 11 shows different sharpening techniques and their differences.

The two parabolic mirrors have focal length of 1524 mm and are located exactly one focal length from the pinhole or the camera. This exact distance insures that the mirrors projects parallel beam of light. The mirror that is closer to the light source projects the parallel light beam to the test area and to the second mirror. The second mirror intercepts the light and form a focused image [13]. The high-speed camera can capture up to 40000 frames/second, which allow us to visualize the different densities of the combustion mixture [12].

Figures 11 through 14 show the outwardly propagating flames that was taken by the high-speed camera. As percentage of CO_2 is increased the flame becomes slower for the same condition.

Figure 11 show that for $\alpha = 0\%$ and $\phi = 0.8$ the flame is faster than $\alpha = 20\%$ and $\alpha = 30\%$. The flame is fastest at fuel equivalence ratio of $\phi = 1.0$ followed by $\phi = 1.2$ for every test set. Figure 12 shows the cellularity of the flame at $P_i = 2$ atm. The flame is highly cellular at the stochiometric ratio. Furthermore, as the percentage of CO_2 is increased the flame becomes less cellular.

Figure 13 shows the flame is smooth at higher temperature and its only effected by the pressure. Figure 14 shows the effect of pressure on cellularity.

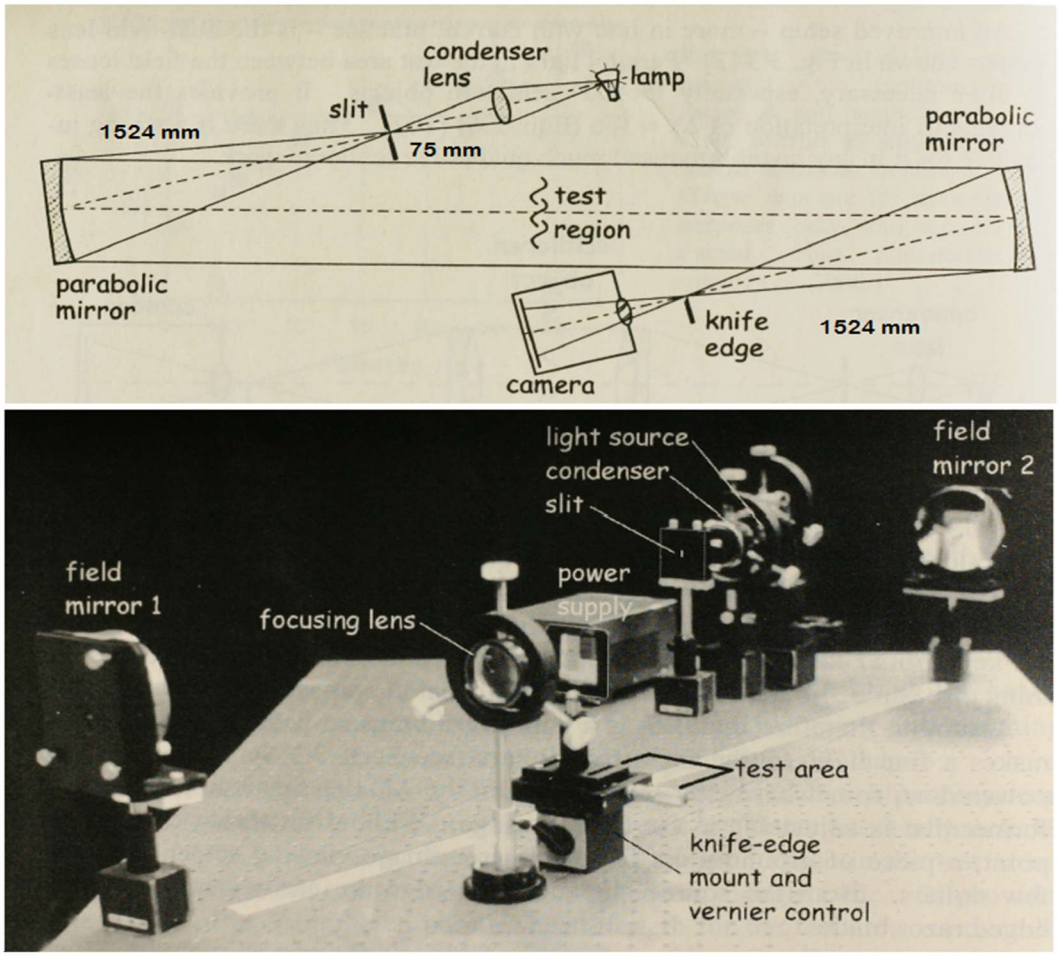

Figure 10: The standard mirror alignment with mirrors z-type

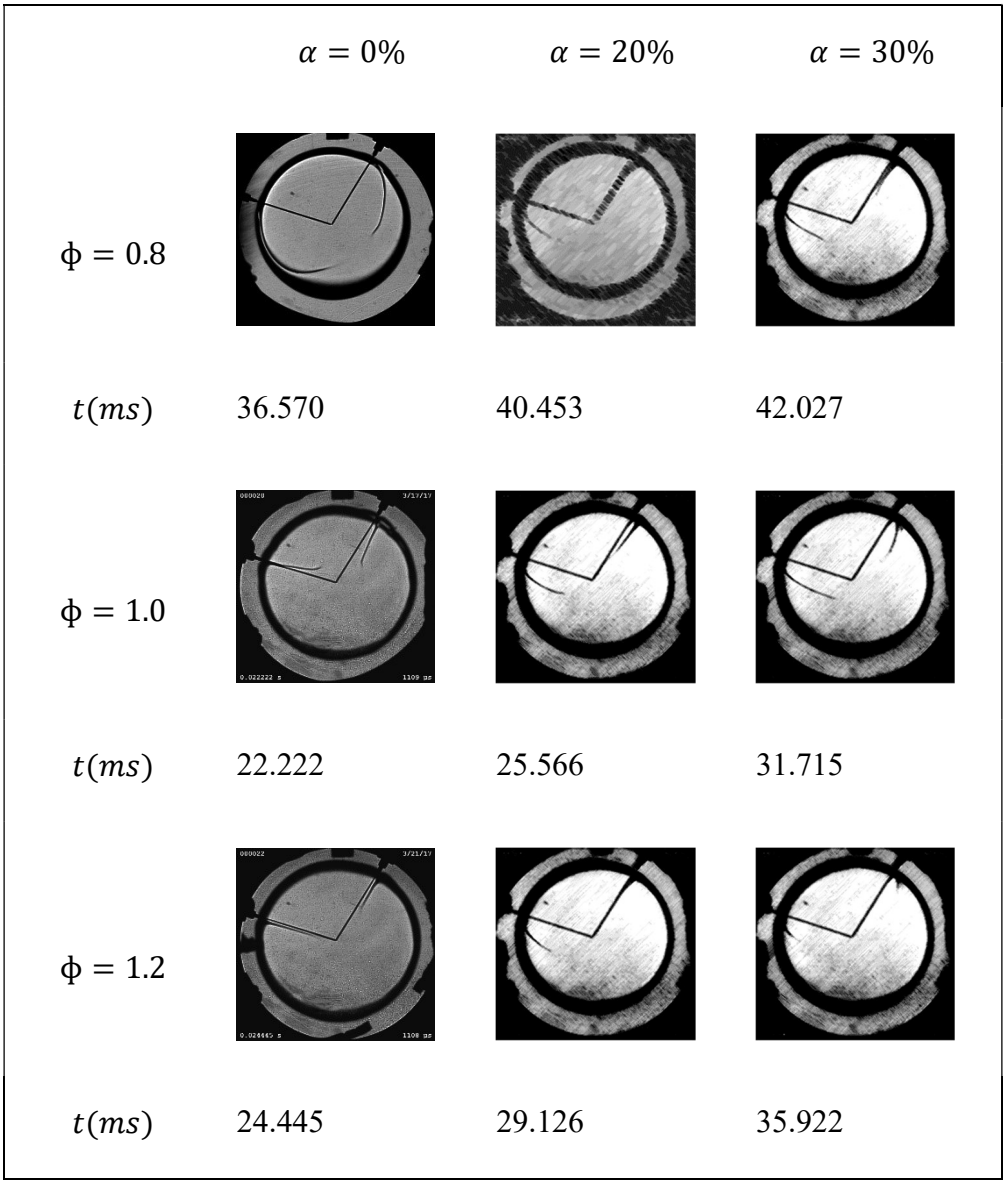

Figure 11: Pictures of the CH_4/air/CO_2 mixtures flames for different equivalence ratios and carbon dioxide percentages (α), initial temperature of 330 K, initial pressure of 1.0 atm, and at the same flame radius

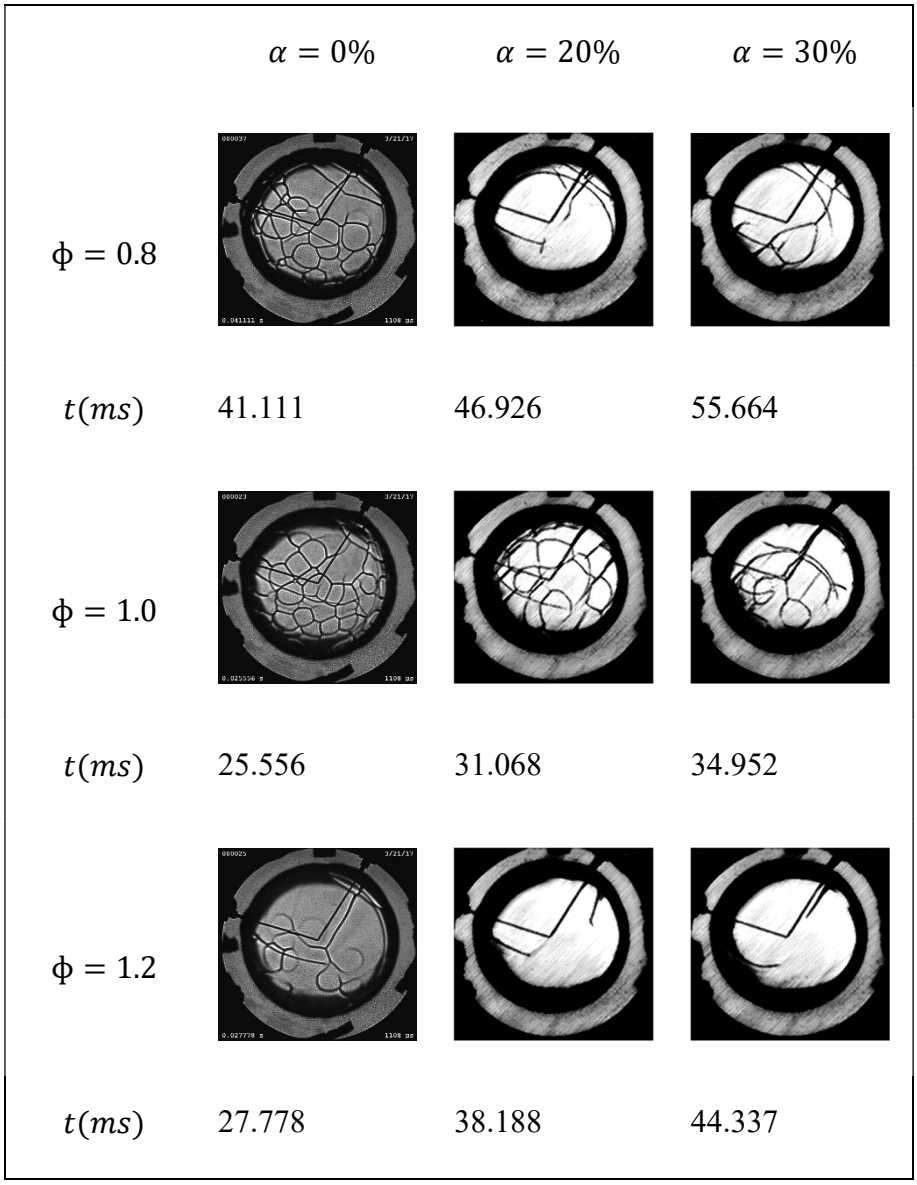

Figure 12:Pictures of the CH_4/air/CO_2 mixtures flames for different equivalence ratios and carbon dioxide percentages(α), initial temperature of 330 K, initial pressure of 2.0 atm, and at the same flame radius

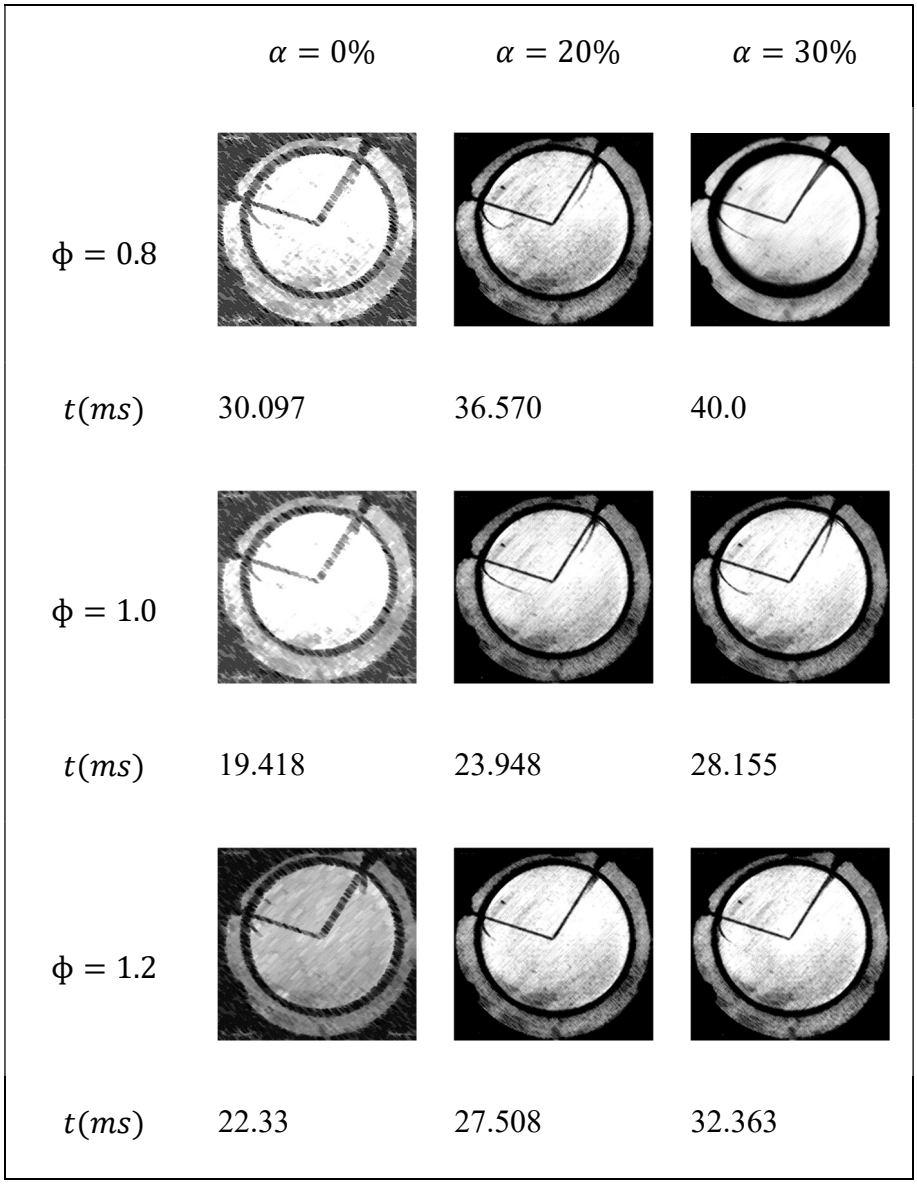

Figure 13:Pictures of the CH_4/air/CO_2 mixtures flames for different equivalence ratios and carbon dioxide percentages (α), initial temperature of 360 K, initial pressure of 1.0 atm, and at the same flame radius

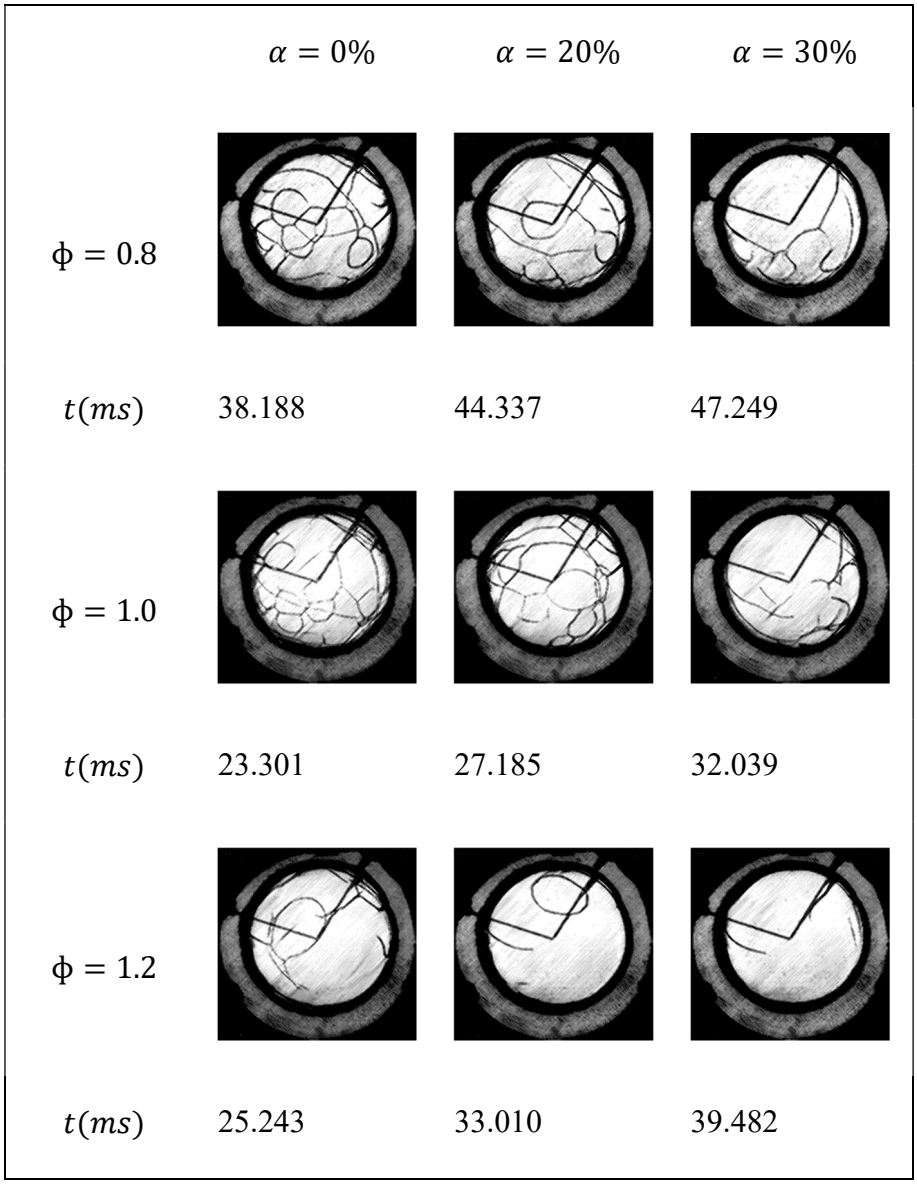

Figure 14:Pictures of the CH_4/air/CO_2 mixtures flames for different equivalence ratios and carbon dioxide percentages (α), initial temperature of 360 K, initial pressure of 2.0 atm, and at the same flame radius

3. Experiment Procedures

3.1. Method of Partial Pressure

The desired partial pressure is calculated using the partial pressure method. In this study experiments were carried out for methane, carbon dioxide, and air mixtures.

For any hydrocarbon, of C_xH_y

$$C_xH_y + \frac{\left(x+\frac{y}{4}\right)}{\emptyset}\,(O_2 + 3.76N_2) \rightarrow xCO_2 + \frac{y}{2}H_2O + 3.76\frac{\left(x+\frac{y}{4}\right)}{\emptyset}N_2 + \left(x+\frac{y}{4}\right)\left(\frac{1}{\emptyset}-1\right)\,O_2 \quad (2)$$

For CH_4/ CO_2 mixture, we have two fuels we need to add α which is the percentages of CO_2 in the mixture.

$$\emptyset\,[\,\alpha CO_2 + (1-\alpha)CH_4] + 2(1-\alpha)(O_2 + 3.76N_2) \rightarrow Products \quad (3)$$

$$X_i = \frac{N_i}{N_{Total}} \quad (4)$$

$$X_{CO2} = \frac{N_{CO2}}{N_{Total}} = \frac{\emptyset\ \alpha}{\emptyset\ \alpha + \emptyset\,(1-\alpha) + 9.52(1-\alpha)} \quad (5)$$

$$X_{CH4} = \frac{N_{CO2}}{N_{Total}} = \frac{\emptyset\,(1-\alpha)}{\emptyset\ \alpha + \emptyset\,(1-\alpha) + 9.52(1-\alpha)} \quad (6)$$

$$X_{Air} = \frac{N_{Air}}{N_{Total}} = \frac{9.52(1-\alpha)}{\emptyset\ \alpha+\emptyset\,(1-\alpha)+9.52(1-\alpha)} \quad (7)$$

$$P_i = X_i P_{total} \quad (8)$$

$$P_{CO_2} = X_{CO_2} P_{total} \quad (9)$$

$$P_{CH_4} = X_{CH_4} P_{total} \quad (10)$$

$$P_{Air} = X_{Air} P_{total} \quad (11)$$

3.2. Preheating and Filling Up

If the experiments were to be carried out at room temperature the filling can be started when the vacuum reading is around 100 millitorr. Otherwise, the chamber must be heated to the desired initial temperature. The process of heating is very important and it will take time to reach steady state. The experimenter start by filling the vessel with the lowest partial pressure, which is CO_2 in this study. Then CH_4 is filled since its partial pressure is higher than that of CO_2. Lastly, the air is filled and the total pressure must be equal to the initial pressure.

3.3. Igniting and Post-Processing.

After the filling is complete the experimenter starts by switching the ignition box capacitor and opening the LabView VI to start igniting the mixture. The waiting time between filling and igniting is very important in order to give the mixture enough time to mix evenly.

The LabView VI will record the Pressure time trace. Figures 18 through 20 show pressure vs time trace. Figures 17 through 19 show the raw data after the experiment. The raw data is further processed to include only the pressure time trace for smooth flames or before it hits the walls of the vessel if the flame is not cellular. In Figure 17, the little notch at the stochiometric mixture indicate that the flame has hit the wall. Figure 18 shows the effect of the addition of 20% CO_2 on the slope of the pressure time trace.

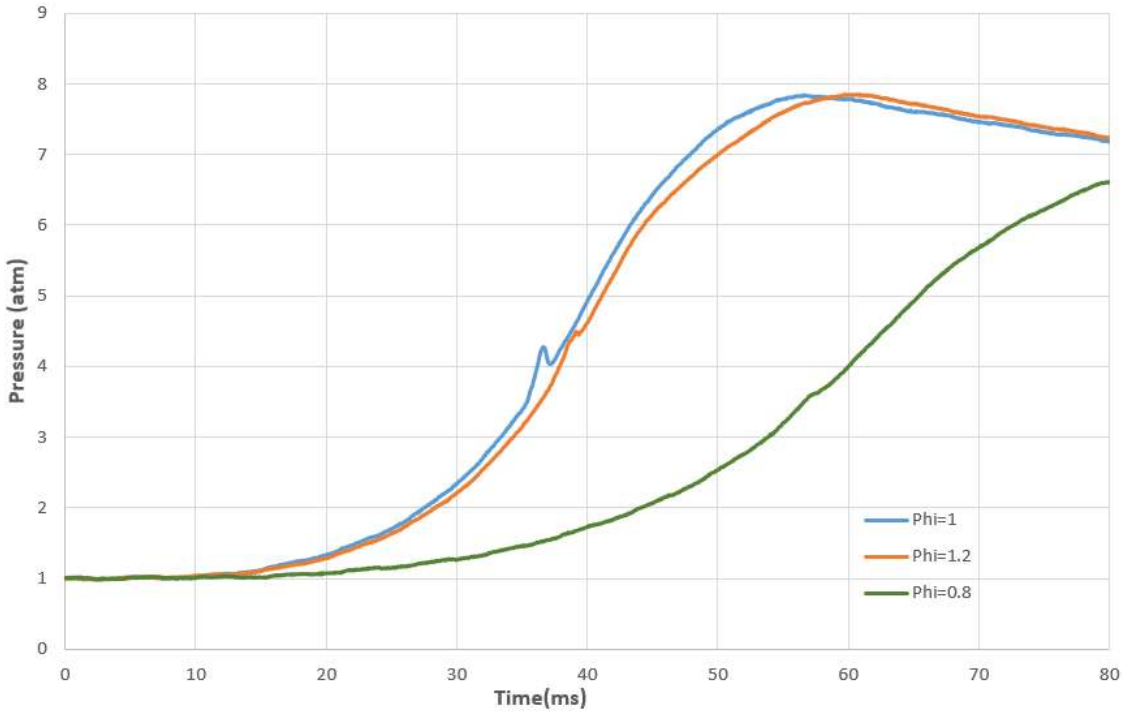

Figure 15: Pressure vs time for mixture of methane/air, at T_i = 298 K, and P_i = 1 atm for three different fuel equivalence ratios of 0.8, 1.0, and 1.2

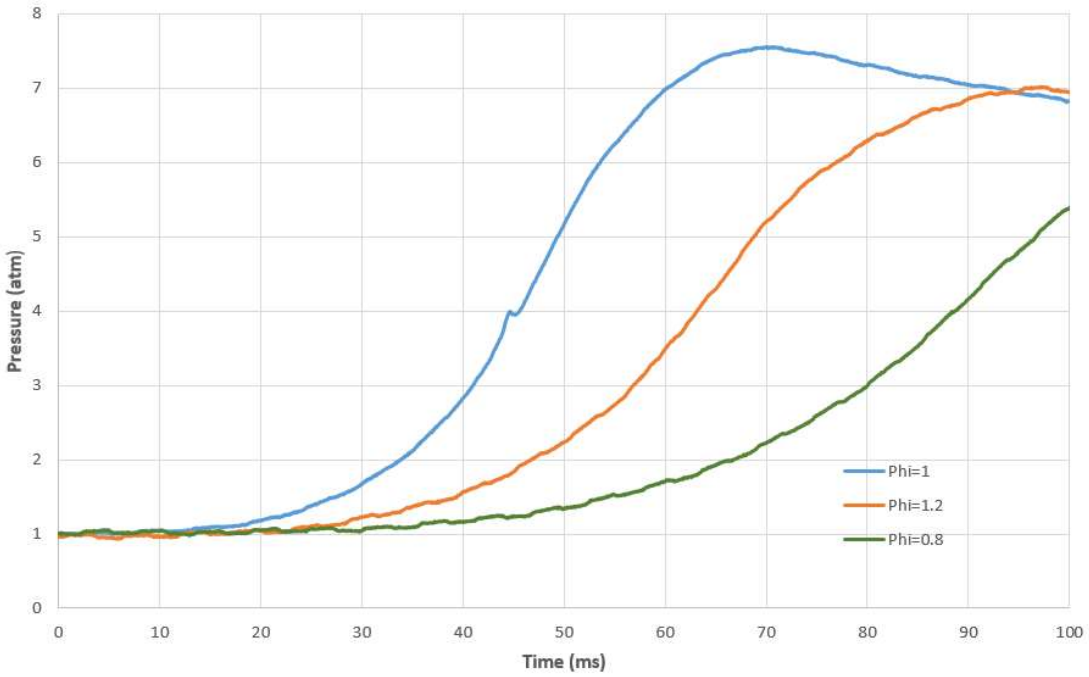

Figure 16: Pressure vs time for mixture of methane/air/ 20% carbon dioxide, at T_i = 298 K, and P_i =1 atm for three different fuel equivalence ratios of 0.8, 1.0, and 1.2

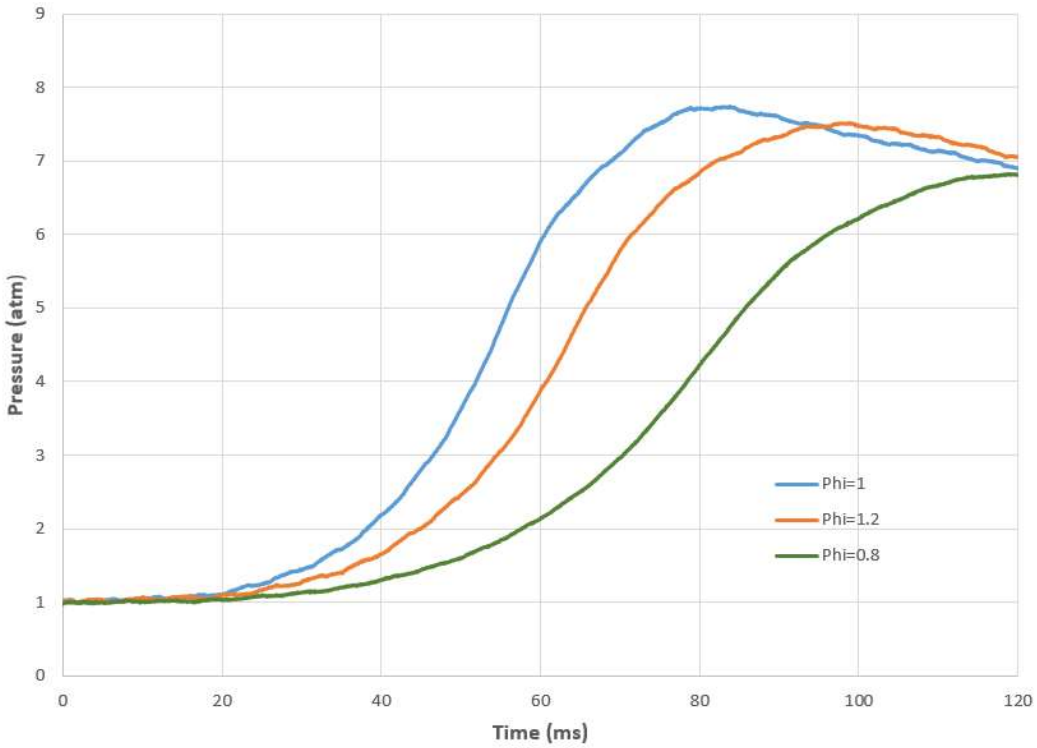

Figure 17: Pressure vs time for mixture of methane/air/ 30% carbon dioxide, at T_i = 298 K, and P_i = 1 atm for three different fuel equivalence ratios of 0.8, 1.0, and 1.2

4. Thermodynamic Model

A thermodynamic model has been developed to calculate burning speed from pressure measurement. In the model burning gas is in the center of vessel surrounded by reaction sheet, pre-heat flame zone, core unburned gas and boundary layer gas touching the vessel as shown in Figure 18. In the spherical flames measured pressure is used along with the mass, energy balance, ideal gas equations to calculate the temperature distribution in the unburned and burned gas region. Also, the mass fraction of the burned gas can be calculated. In the model, all gases behave as ideal gases with the following equations.

$$pv = RT \tag{12}$$

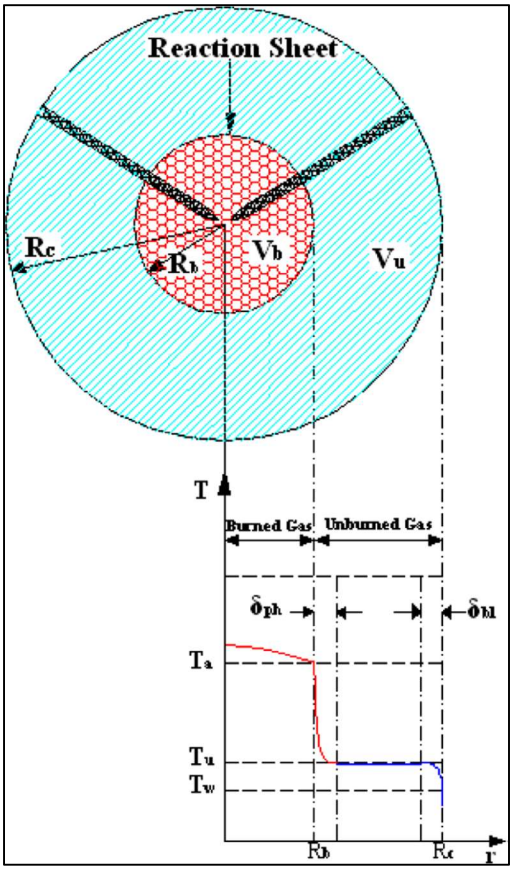

Figure 18:Schematic of three different zones in the thermodynamics model

Where, p is the pressure which is measured within the chamber, v is the specific volume, R is the specific gas constant, and T is the temperature.

The mass balance equation for the burned and unburned gas region is

$$m = m_b + m_u = \rho_b V_b + \rho_u V_u = p_i(V_c - V_e)/RT_i \quad (13)$$

where m is the total mass of the chamber, m_b is the mass of the burned gas zone, m_u is the mass of the unburned gas zone, V_c is the volume of the chamber and V_e is the volume of the spark electrodes. In this equation, the subscript i denotes the initial conditions, and subscripts b and u represent the burned gas and unburned conditions respectively. And ρ is the average density and V is the volume of the gas. The total volume of the gas in the combustion chamber is

$$V_i = V_c - V_e = V_b + V_u \quad (14)$$

where

$$V_b = \int_0^{m_b} v'(T', p)\, dm' = \int_0^{m_b} v'_{bs}(T', p)\, dm' - V_{eb} \quad (15)$$

V_b is the volume of the burned gas, v_{bs} is the specific volume of isentropically compressed burned gas.

$$V_{eb} = \int_{eb}(v'_{bs} - v')\, dm' \quad (16)$$

$V_{eb}$is the displacement volume of the electrode boundary layers.

$$V_u = \int_{m_b}^{m} v'(T', p)\, dm' = m(1 - x_b)v_{us} - V_{wb} - V_{ph} \quad (17)$$

V_u is the volume of the unburned gas, $x_b = m_b/m$ is the burned gas mass fraction, v_{us} is the specific volume of the isentropically compressed unburned gas,

$$V_{wb} = \int_{wb}(v_{us} - v')\, dm' \tag{18}$$

V_{wb} is the displacement volume of the wall boundary layer, and

$$V_{ph} = \int_{ph}(v_{us} - v')\, dm' \tag{19}$$

V_{ph} is the displacement volume of the preheat zone ahead of the reaction layer.

The energy balance equation is given by

$$E_i - Q_e - Q_w - Q_r = E_b + E_u \tag{20}$$

where E_i is the initial energy of the gas, Q_e is the conductive energy loss to the electrodes, Q_w is the energy loss to the wall, Q_r is the radiation energy loss,

$$E_b = \int_0^{m_b} e'(T', p)\, dm' = \int_0^{m_b} e'_{bs}(T', p)\, dm' - E_{eb} \tag{21}$$

E_b is the energy of the burned gas, e_{bs} is the specific energy of isentropically compressed burned gas,

$$E_{eb} = \int_{eb}(e'_{bs} - e')\, dm' \tag{22}$$

E_{eb} is the energy defect of the electrode boundary layer,

$$E_u = \int_{m_b}^{m} e'(T', p)\, dm' = m(1 - x_b)e_{us} - (E_{wb} + E_{ph}) \tag{23}$$

E_u is the energy of the unburned gas, e_{us} is the specific energy of the isentropically compressed unburned gas,

$$E_{wb} = \int_{wb}(e_{us} - e')\, dm' \tag{24}$$

$E_{wb}$is the energy defect of the wall boundary, and

$$E_{ph} = \int_{ph}(e_{us} - e')\, dm' \tag{25}$$

E_{ph} is the energy defect of the preheat layer.

The definition of enthalpy

$$h = h_f + \int_0^T C_p\, dT = e + pv \tag{26}$$

Using ideal gas assumption, constant specific heat

$$e - h_f = \int_0^T C_p\, dT - pv = C_p T - pv \tag{27}$$

$$C_p - C_v = R \tag{28}$$

$$\frac{C_p}{C_v} = \gamma \tag{29}$$

Combining Equation (26) with Equations (27) and (28), we get equation (29)

$$e - h_f = pv/(\gamma - 1) \tag{30}$$

where h_f is the enthalpy of formation of the gas at zero degrees Kelvin and γ is the specific heat ratio. By this relation, Equations (22), (24), and (25) can be written as

$$E_{eb} = \int_{eb}\left(\frac{pv_{bs}}{r_b - 1} + h_f - \left(\frac{pv'}{r_b - 1} + h_f\right)\right)dm' \tag{31}$$

$$E_{eb} = \frac{p\int_{eb}(v_{bs} - v')dm'}{\gamma_b - 1} = pV_{eb}/(\gamma_b - 1) \tag{32}$$

$$E_{wb} = \int_{wb}\left(\frac{pv_{us}}{r_u - 1} + h_f - \left(\frac{pv'}{r_u - 1} + h_f\right)\right)dm' \tag{33}$$

$$E_{wb} = \frac{p\int_{wb}(v_{us} - v')dm'}{\gamma_u - 1} = pV_{wb}/(\gamma_u - 1) \tag{34}$$

$$E_{ph} = \int_{ph}\left(\frac{pv_{us}}{r_u - 1} + h_f - \left(\frac{pv'}{r_u - 1} + h_f\right)\right)dm' \tag{35}$$

$$E_{ph} = \frac{p\int_{ph}(v_{us} - v')dm'}{\gamma_u - 1} = pV_{ph}/(\gamma_u - 1) \tag{36}$$

the compression work terms on the boundary layer may be neglected and the resulting equations are

$$Q_e = \frac{pV_{eb}}{\gamma_b - 1} = E_{eb} \tag{37}$$

$$Q_w = \frac{pV_{wb}}{\gamma_u - 1} = E_{wb} \tag{38}$$

The radiation energy loss from the burned gas was calculated using

$$Q_r = \int_0^t \dot{Q}_r\,(t')dt' = 4\alpha_p V_b \sigma T_b^4 \tag{39}$$

where α_p is the Planck mean absorption coefficient and σ is the Stefan-Boltzman constant.

Finally, combining Equations (14), (15), and (17) gives

$$\int_0^{x_b}(v_{bs}(T',p)-v_{us})\,dx' = v_i - v_{us} + (V_{eb}+V_{wb}+V_{ph})/m \tag{40}$$

and combining Equations (11), (12), and (14) gives

$$\int_0^{x_b}(e_{bs}(T',p)-e_{us})\,dx' =$$

$$e_i - e_{us} + \frac{\frac{pV_{ph}}{\gamma_u-1}-Q_r}{m} - A_{wb}(p\delta_{wb}-\int_0^p \delta_{wb}dp) - A_{eb}(p\delta_{eb}-\int_0^p \delta_{eb}dp) \tag{41}$$

where $v_i = (V_c - V_e)/m$ and $e_i = E_i/m$ are the initial specific volume and energy of the unburned gas in the chamber.

The above two Equations (41) and (42) have been solved for two unknowns: burned mass fraction, $x_b(t)$, and the burned gas temperature of the last layer, $T_b(r,t)$. Given pressure, $p(t)$, as a function of time, they can be solved numerically using Newton-Raphson method to obtain the burned mass fraction as a function of time and temperature distribution.

Laminar burning speed can be defined as

$$S_u = \frac{\dot{m_b}}{\rho_u A_b} = \frac{m\dot{x_b}}{\rho_u A_b} \tag{42}$$

where

$$A_b = 4\pi r_b^2 - 2\pi r_e^2 \tag{43}$$

$$V_b = \frac{4}{3}\pi r_b^3 - 2\pi r_e^2 r_b \tag{44}$$

A_b is the area of a sphere having a volume equal to that of the burned gas and $x_b(t)$ can be solve from the previous equations. This expression is valid for smooth, cracked, or wrinkled flames of any shape. Thus, laminar burning speed can be calculated from equation 42.

5. Results and Discussion

Experiments were conducted for the 54 conditions in Table 1 and laminar burning speeds were measured for smooth flames and with radii larger than 4 cm. Figures from 22 through 39 present the measured LBS for ϕ = 0.8, 1.0, and 1.2 at a given initial condition. Each condition show results of LBS for isentrope.

It is noticed from Figures 22 through 24 that the LBS decreases as the percentage of carbon dioxide is increased. For example, for Xco_2 = 0% and ϕ = 1.0, LBS is measured to be 38 cm/s vs 29 cm/s at Xco_2 = 20% and 23 cm/s for Xco_2 = 30%. The decrease of LBS between Xco_2 = 0% and Xco_2 = 20% is 9 cm/s whereas between Xco_2 = 20% and Xco_2 = 30% the decrease is only 6 cm/s.

When ϕ = 1.2 the decrease is almost the same between Xco_2 = 0% and Xco_2 = 20%. (i.e., LBS is 35 cm/s for Xco_2 = 0% and 27 cm/s for Xco_2 = 20% with 8 cm/s decrease). Moreover, the decrease is exactly 6 cm/s for ϕ = 1.2 between Xco_2 = 20% and Xco_2 = 30% with measured LBS of 27 cm/s and 21 cm/s respectively. The decrease for ϕ = 0.8 between Xco_2 = 0% and Xco_2 = 20% is also 9 cm/s. (i.e., from 30 cm/s to 21 cm/s). However, the decrease between Xco_2 = 20% and Xco_2 = 30% is only 2 cm/s but it's similar to the decrease of the measurements reported in [3].

As T_i is increased from 298 K to 330 K, the LBS decrease between different diluent concentration is almost maintained for $\phi = 1.2$ and $\phi = 0.8$ (i.e., the decrease between $Xco_2 = 0\%$ and $Xco_2 = 20\%$ for $\phi = 0.8$ is 7 cm/s from 35 cm/s to 28 cm/s and the decrease is 6 cm/s between $Xco_2 = 20\%$ and $Xco_2 = 30\%$ for $\phi = 0.8$ from 28 cm/s to 22 cm/s respectively). For $\phi = 1.0$ the decrease is about 5 cm/s between $Xco_2 = 0\%$ and $Xco_2 = 20\%$ with measured LBS of 42 cm/s and 27 cm/s respectively.

The decrease of LBS between $Xco_2 = 0\%$ and $Xco_2 = 20\%$ becomes smaller as T_i increased from 330 K to 360 K, as shown in Figures 28 through 30. For example, when $\phi = 0.8$ and $Xco_2 = 0\%$ LBS is measured to be 34 cm/s compared to 29 cm/s when $Xco_2 = 20\%$.

Figures 31 through 39 represent LBS for $T_i = 298$ K, 330 K, and 360 K for higher initial pressure of 2 atm. The effect of increasing the pressure is noticeable in decreasing LBS but the effect of increasing the CO_2 percentage is still applicable as it decreases the LBS as well. For example, when $\phi = 1.0$ and $Xco_2 = 0\%$ LBS are measured to be 29 cm/s,34 cm/s, and 39 cm/s for $T_i = 298$ K, 330 K, and 360 K respectively. And when $\phi = 1.0$ and $Xco_2 = 20\%$ LBS are measured to be 23 cm/s, 27 cm/s, and 35 cm/s for $T_i = 298$ K, 330 K, and 360 K respectively.

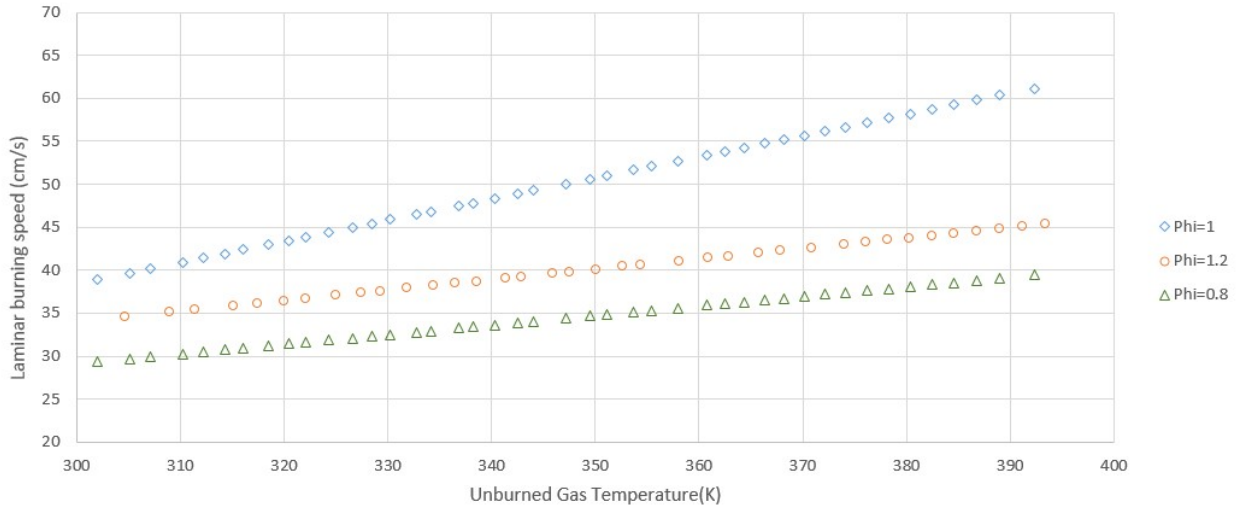

Figure 19: Laminar Burning Speed for of methane, T_i = 298 K, and P_i = 1 atm

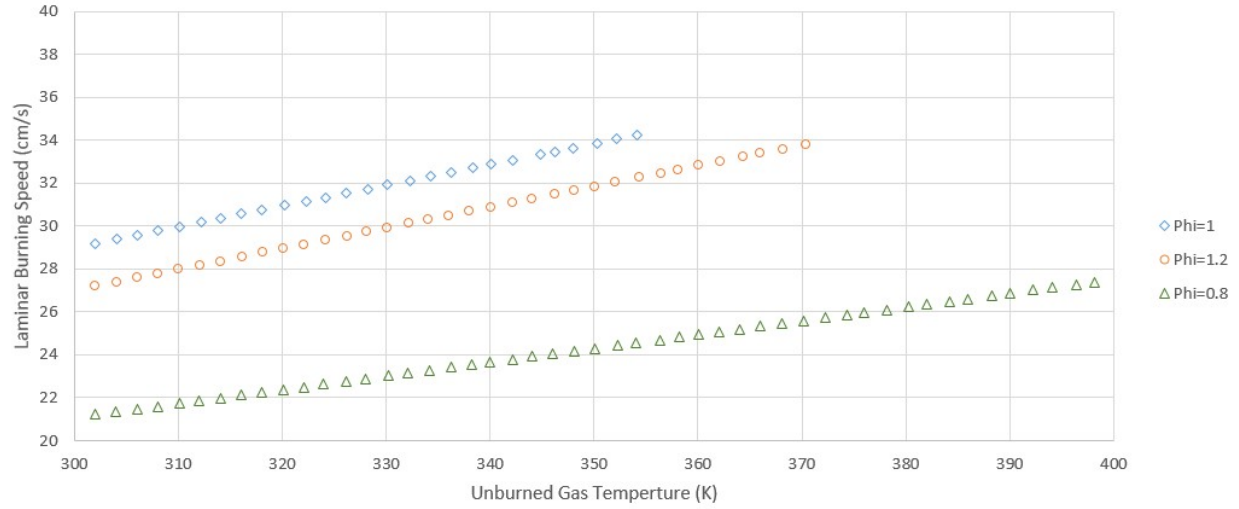

Figure 20: Laminar Burning Speed for mixture of methane and 20% Carbon dioxide, T_i = 298 K, and P_i = 1 atm

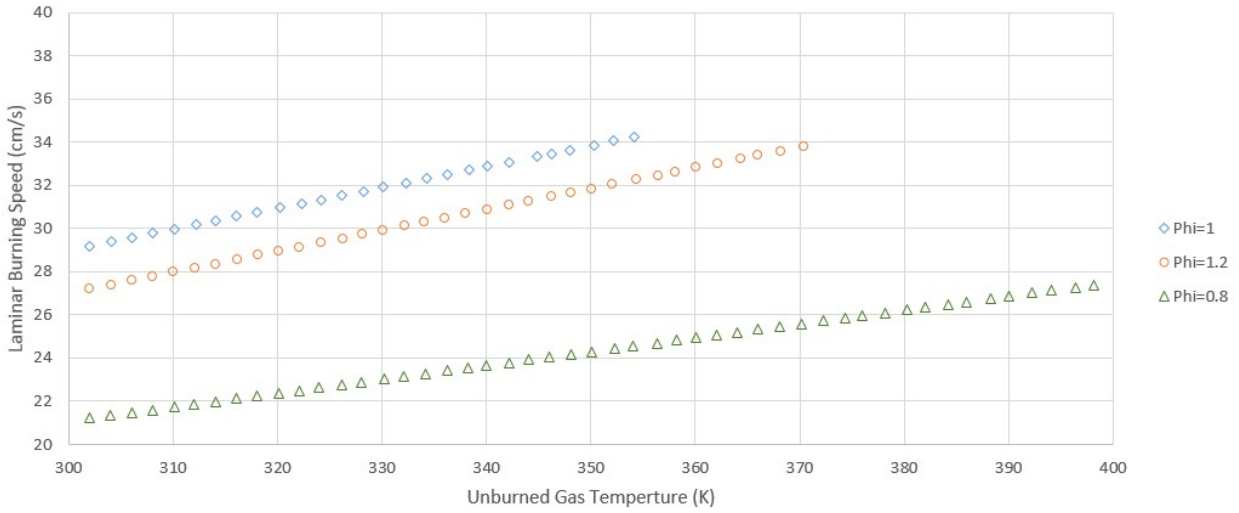

Figure 21: Laminar Burning Speed for mixture of methane and 30% Carbon dioxide, T_i = 298 K, and P_i = 1 atm

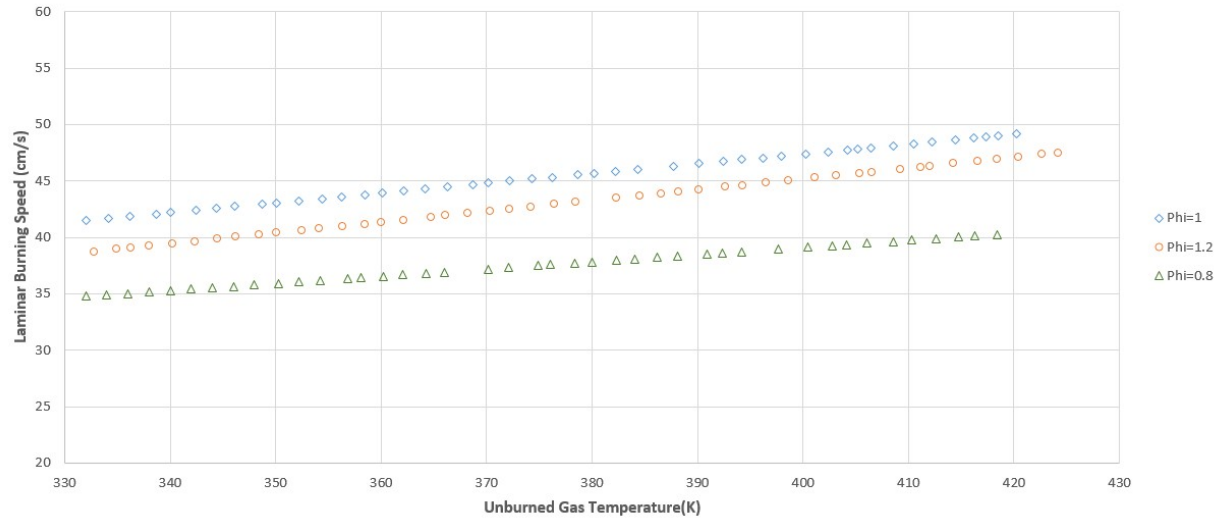

Figure 22: Laminar Burning Speed for of methane, T_i = 330 K, and P_i = 1 atm

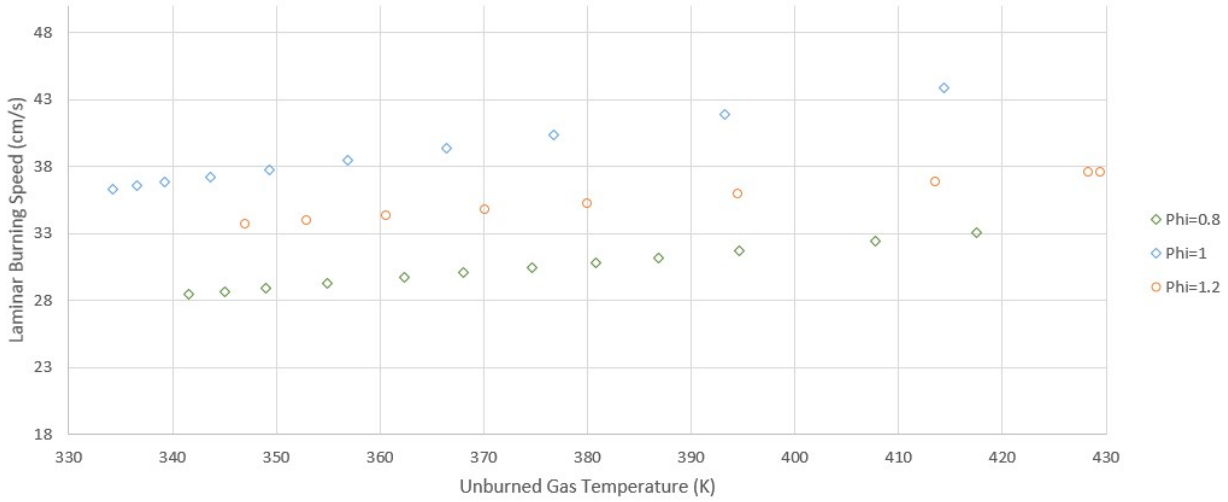

Figure 23: Laminar Burning Speed for mixture of methane and 20% Carbon dioxide, T_i = 330 K, and P_i = 1 atm

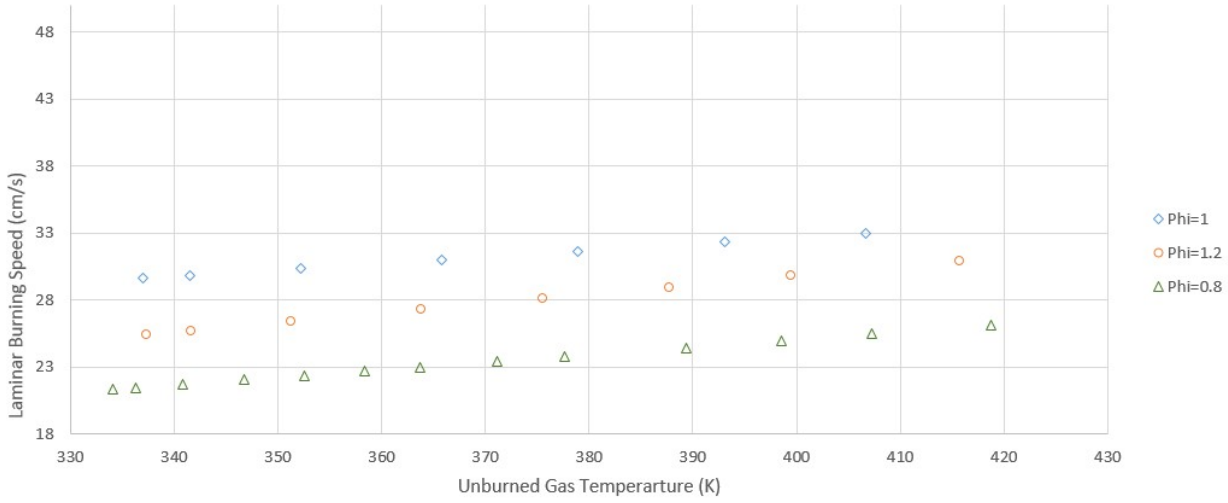

Figure 24: Laminar Burning Speed for mixture of methane and 30% Carbon dioxide, T_i = 330 K, and P_i = 1 atm

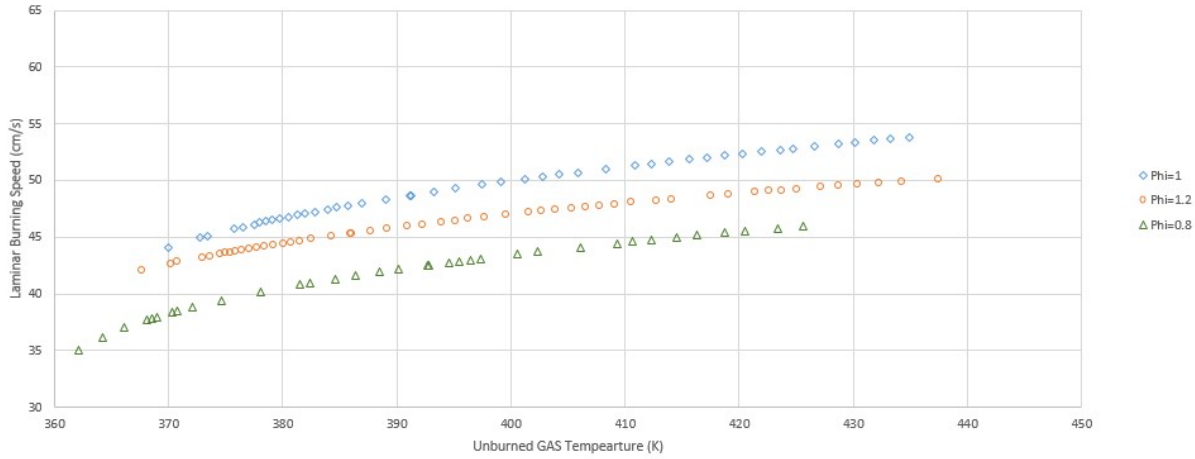

Figure 25: Laminar Burning Speed for of methane, T_i = 360 K, and P_i = 1 atm

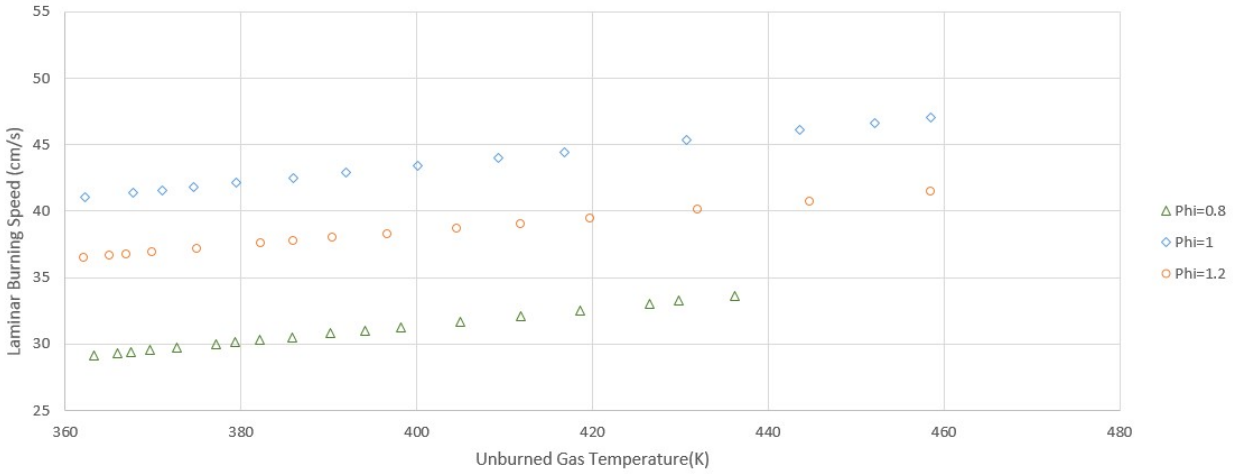

Figure 26: Laminar Burning Speed for mixture of methane and 20% Carbon dioxide, T_i = 360 K, and P_i = 1 atm

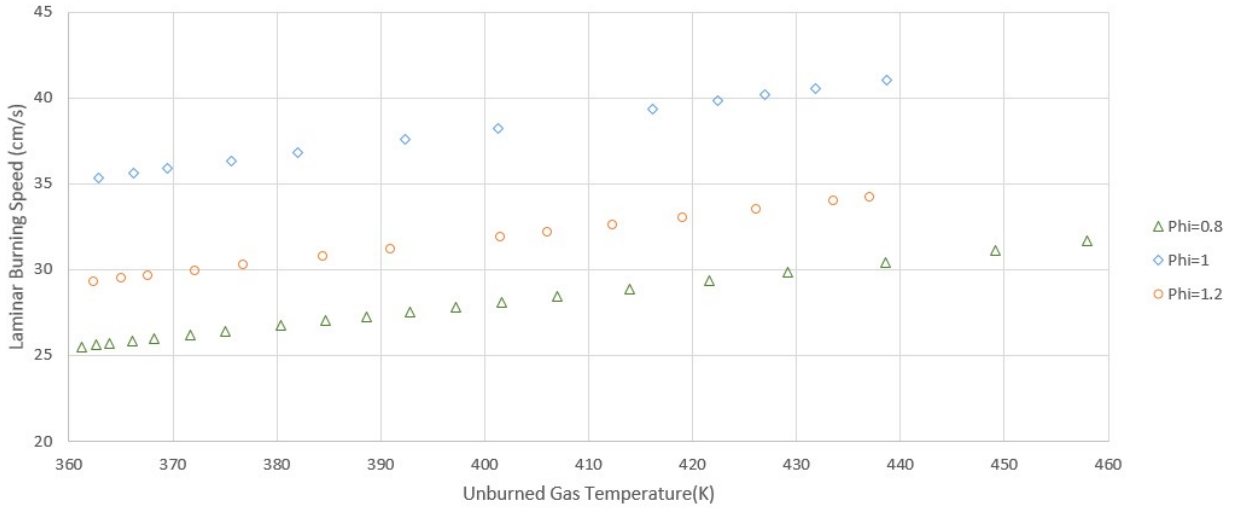

Figure 27: Laminar Burning Speed for mixture of methane and 30% Carbon dioxide, T_i = 360 K, and P_i = 1 atm

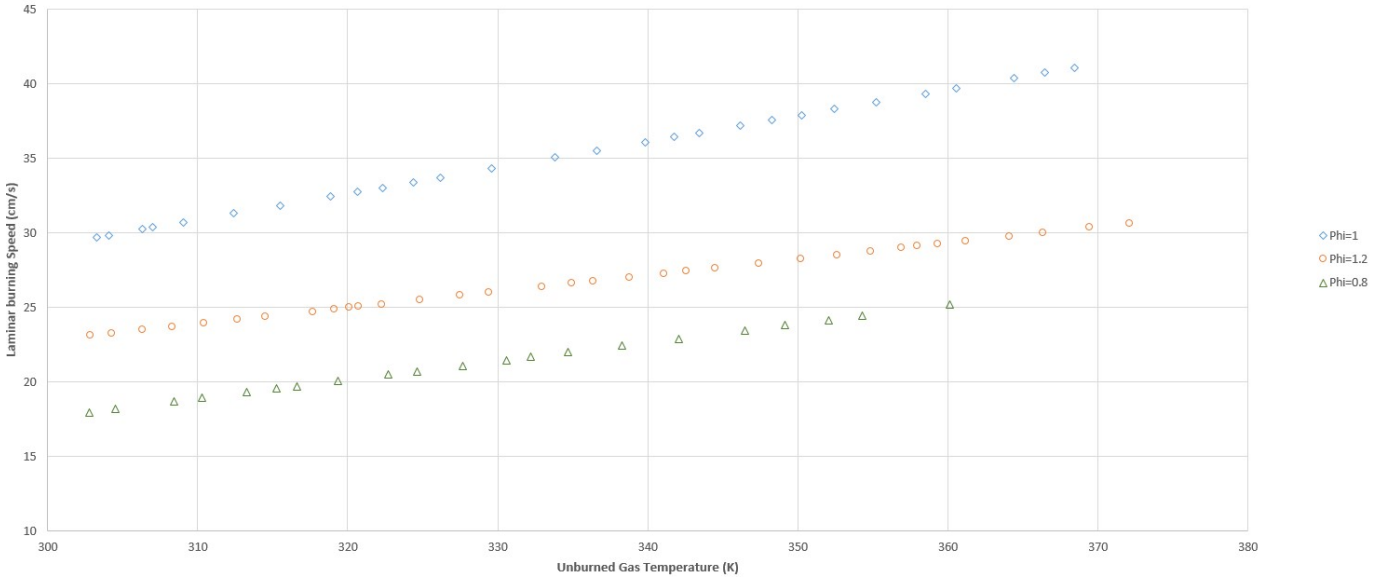

Figure 28: Laminar Burning Speed for of methane, T_i = 298 K, and P_i = 2 atm

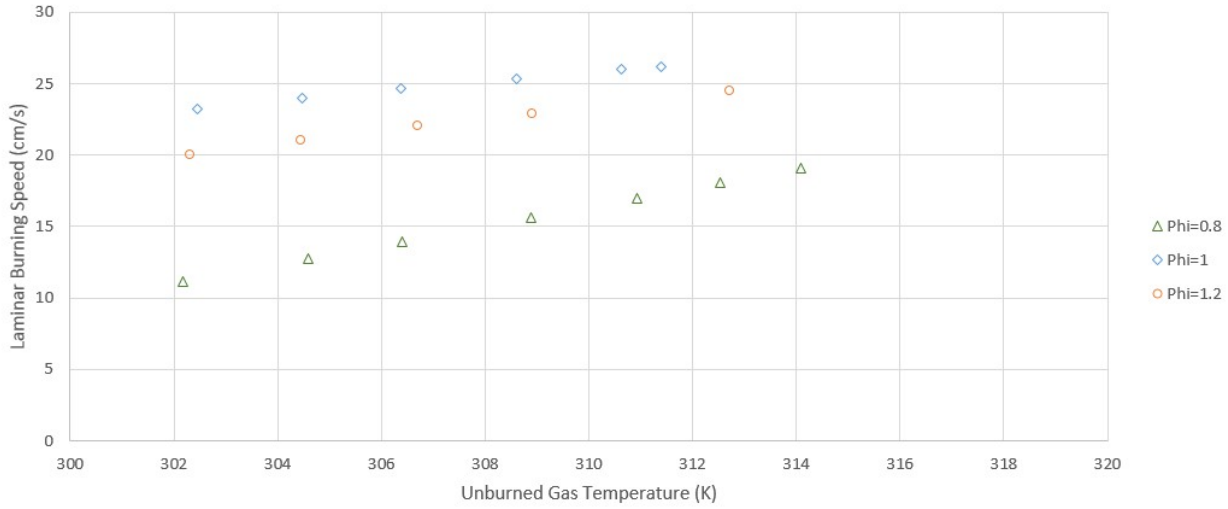

Figure 29: Laminar Burning Speed for mixture of methane and 20% Carbon dioxide, T_i = 298 K, and P_i = 2 atm

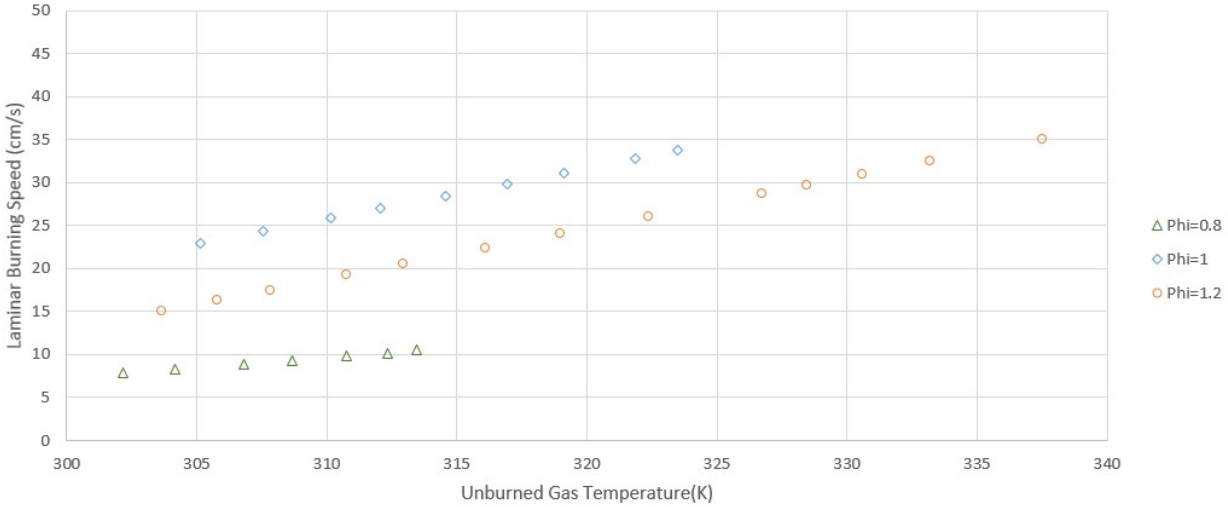

Figure 30: Laminar Burning Speed for mixture of methane and 30% Carbon dioxide, T_i = 298 K, and P_i = 2 atm

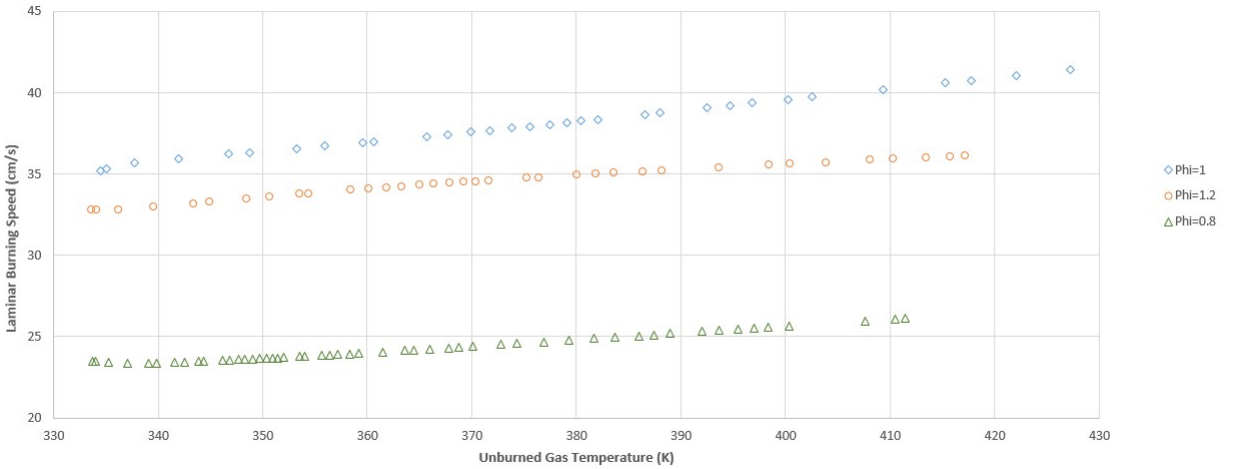

Figure 31: Laminar Burning Speed for of methane, T_i = 330 K, and P_i = 2 atm

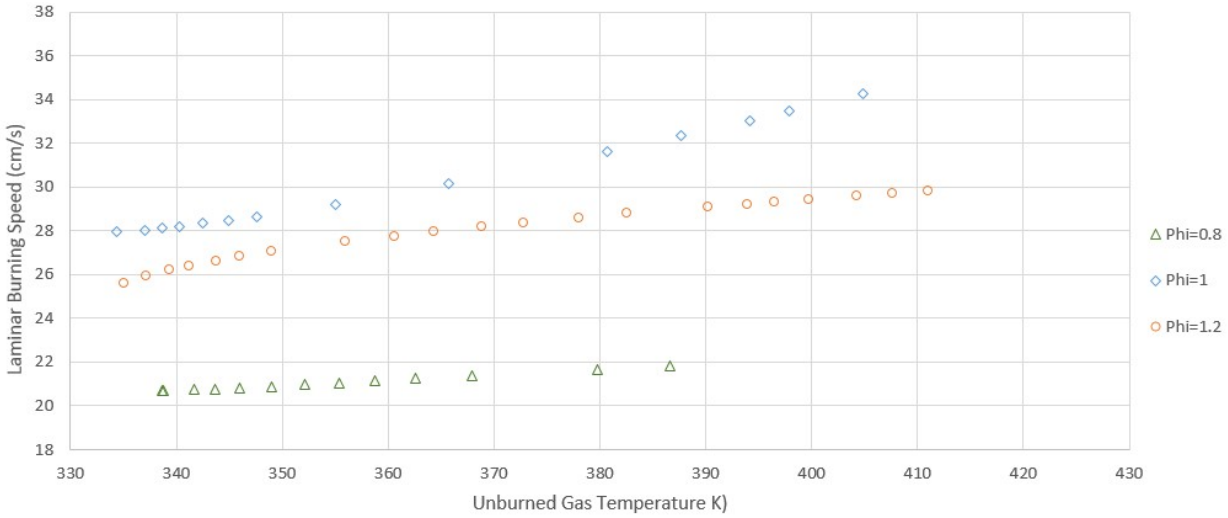

Figure 32: Laminar Burning Speed for mixture of methane and 20% Carbon dioxide, T_i = 330 K, and P_i = 2 atm

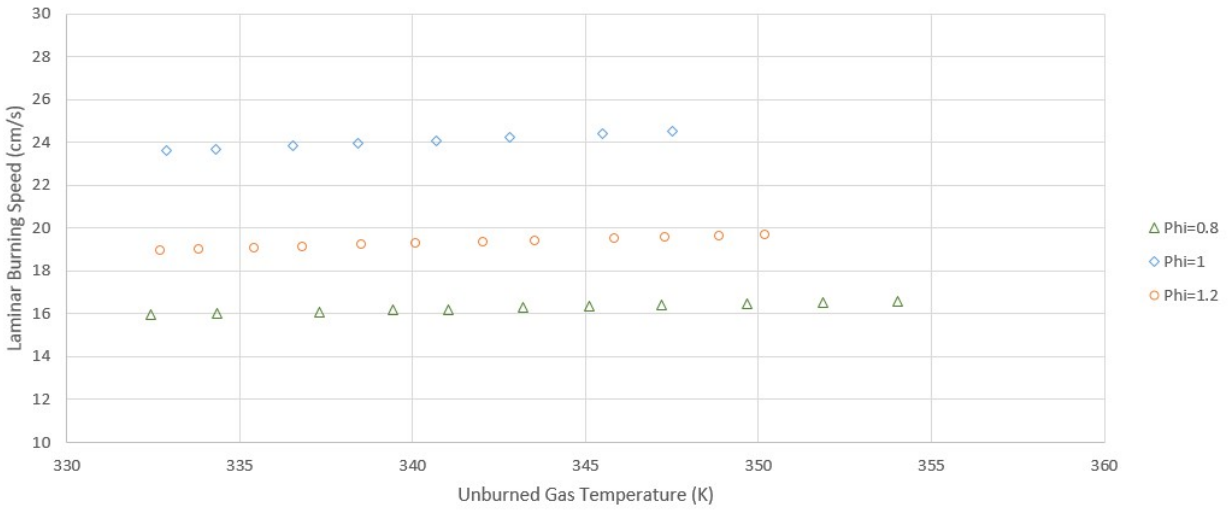

Figure 33: Laminar Burning Speed for mixture of methane and 30% Carbon dioxide, T_i = 330 K, and P_i = 2 atm

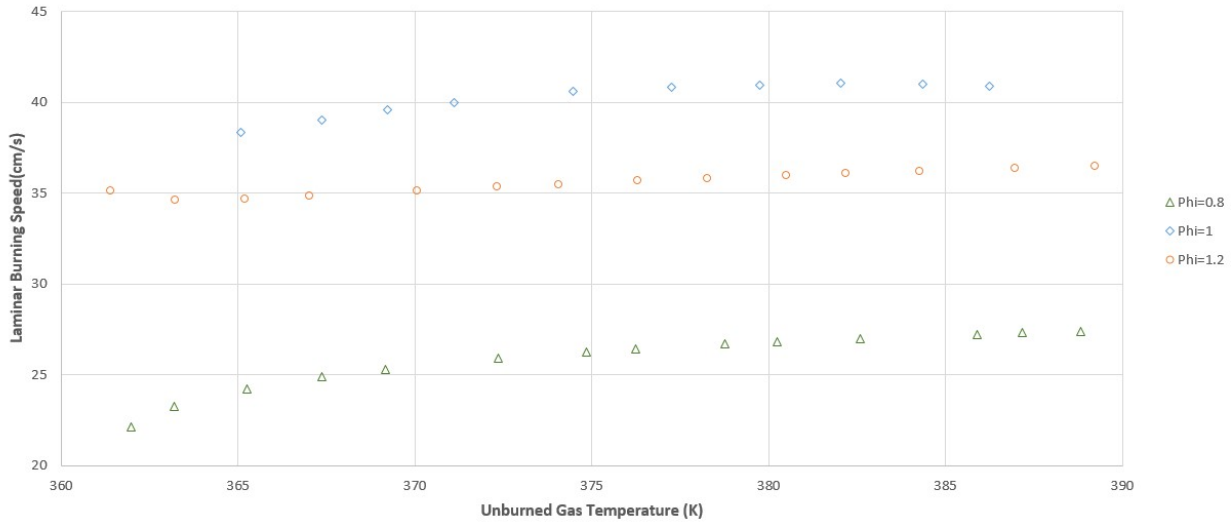

Figure 34: Laminar Burning Speed for of methane, T_i = 360 K, and P_i = 2 atm

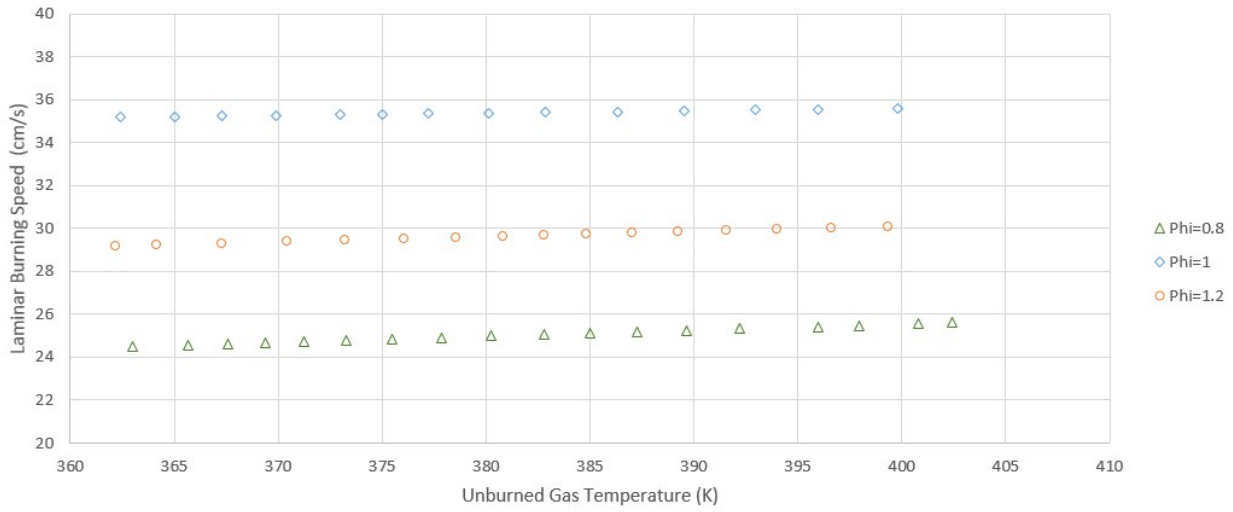

Figure 35: Laminar Burning Speed for mixture of methane and 20% Carbon dioxide, T_i = 360 K, and P_i = 2 atm

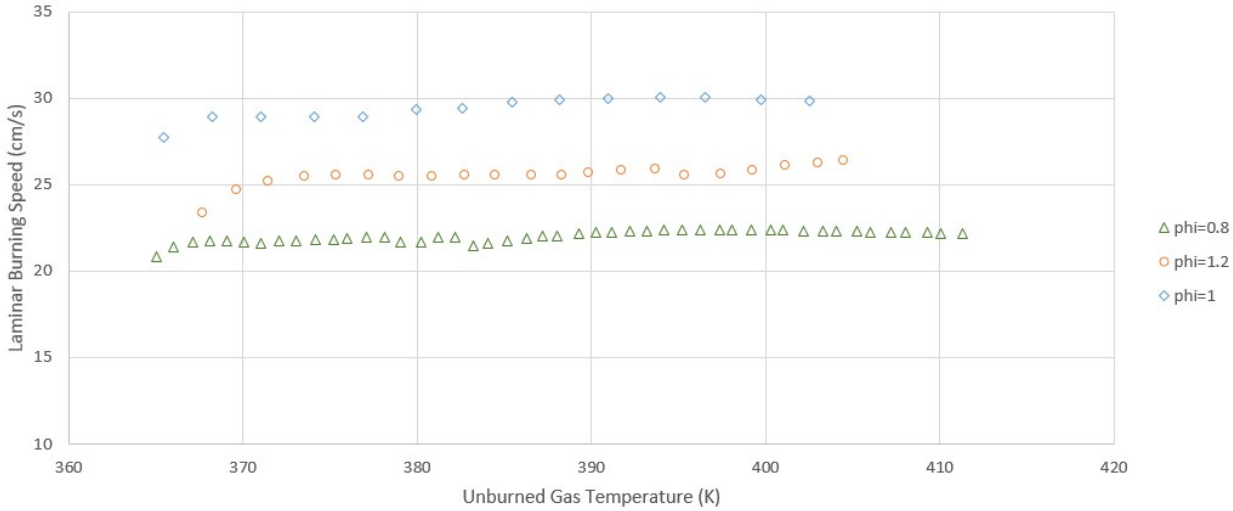

Figure 36: Laminar Burning Speed for mixture of methane and 30% Carbon dioxide, T_i = 360 K, and P_i = 2 atm

6. Conclusion and Recommendation

The laminar burning speed and the flame cellularity of spherically expanding flames of CH_4/air/CO_2 mixtures that have three different carbon dioxide concentrations (0%, 20% and 30%) have been studied for three fuel air equivalence ratios of ϕ = 0.8,1.0, and 1.2. Moreover, three initial temperatures T_i = 298 K, 330 K, and 360 K respectively as well as two initial pressures of P_i = 1 atm and 2 atm. Laminar burning speed measurements covered a wide range of temperatures and pressures up to 430 K and 3.6 atm. Laminar burning speeds of stochiometric mixtures ratios are measured to be the fastest followed by ϕ = 1.2 and ϕ = 0.8. Moreover, LBS is directly proportional to temperature and inversely proportional to pressure. The flame become cellular for P_i = 2 atm and ϕ = 1.0 and less cellular for ϕ = 1.2. The flame cellularity is delayed as the percentage of carbon dioxide is increased.

Future researchers can simulate Biogas and LFG more accurately if the small percentages of carbon monoxide is considered. Moreover, experiment at higher pressures and temperatures than 430 K and 2 atm. can be done to measure the laminar burning speeds of the simulated land fill gas over large range of temperatures, pressures, and fuel air equivalence ratios.

7.References

[1] F. Parsinejad, "Experimental and Theoretical Studies on Flame Propagation and Burning Speeds of JP-8, JP-10 and Reformed Fuels at HighTemperatures and Pressures," Northeastern University, Boston, 2005.

[2] J. C. Oefelein and V. Yang, "Combustion Science and Technology," vol. 178, no. 1-3, pp. i-iii, 2006.

[3] L. Pizzuti n, C.A.Martins,P.T.Lacava, "Laminar burning velocity and flammability limits in biogas: A literature review," *Renewable and Sustainable Energy Reviews,* vol. 62, pp. 856-865, 2016.

[4] Z. Wang, "Measurements of Laminar Burning Speeds and Flame Instability of Syngas/Oxygen/Helium Premixed Flames," ProQUEST, Boston, 2016.

[5] Qin W,EgolfopoulosFN,TsotsisTT, "Fundamental and environmental aspects of landfill gasutilization for power generation," *ChemEng,* vol. 82, p. 157–72., 2001.

[6] Nathan Hinton , Richard Stone, "Laminar burning velocity measurements of methane and carbon dioxide mixtures (biogas) over wide ranging temperatures and pressures," *Fuel,* vol. 114, pp. 743-750, 2014.

[7] "Owner's Manual for Duoseal Vacuum Pumps Models:1402N, 1402N-01, 1402N-10, 1402N-50, 1402N-53,1402N-60, 1402N-63, 1402N-90 & 6D735," Welch-Ilmvac, Niles, IL,

2008.

[8] A. Moghaddas, "Laminar Burning Speed Measurment,Autoignition and Flame Structure Study of Spherically Expanding Flames," Northeastern University, Boston, 2015.

[9] M. Metghalchi, "Laminar Burning Velocity of Mixtures of Air with Indolene,Isooctane,Methanol and Propane," Massatchusetts Institute of Technology , Boston, 1977.

[10] M. Metghalchi, "Laminar Burning Velocity of Isooctane-Air, and Methanol-Air Mixtures at High Temperature and Pressure.," Massachusetts Institute of Technology, Boston, 1976.

[11] O. Mannaa, M. S. Mansour, W. L. Roberts and S. H. Chung, "Laminar burning velocities at elevated pressures for gasoline and gasoline surrogates associated with RON," *Combustion and Flame,* vol. 162, no. 6, p. 2311–2321, 2015.

[12] N. Degen, "An Overview on Schlieren Optics and its Applications," Swiss Federal Institute of Technology (ETH) , Zurich, 2012.

[13] A. Davidhazy, "Introduction to shadowgraph and schlieren imaging," 2006. [Online]. Available: http://scholarworks.rit.edu/article/478.

[14] C. Bennett, "Laminar Burning Speed and Flame Structure of 1,1-Difluoroethane (HFC-152A)/Air and Difluoromethane (HFC-32)/Air Mixtures," Northeastern University, Boston, 2011.

[15] A. W. Ahlholm, "An Investigation of the Flame Structures and Burning Speeds of

H2/CO/Air Mixtures," Northeastern University, Boston, 2015.

[16] B. N. Alhazmi, "Measurement of Laminar Burning Speed and Investigation of Flame Stability of Syngas/Air Mixture," Northeastern University, Boston, 2015.

[17] E. Rokni, "Measurement of Laminar Burning Speeds and Investigation of Flame Stability of Acetylene (C2H2)/air Mixtures," Northeastern University, Boston, 2014.

[18] B. Lewis and G. v. Elbe, Combustion Flames and Explosions of Gases 2nd Edition, Pittsburgh,PA and Alexandria,VA: Academic Press, 1967.

[19] K. Vien, Experiments on the Effect of Exhaust Gas Recirculation Diluent on the Laminar Burning Speed and Stability of Syngas/Air flames, Boston: Northeastern University, 2016.

[20] K. Kumar and C. J. Sung, "Laminar flame speeds and extinction limits of preheated," *Combustion and Flame,* pp. 209-244, 2007.

[21] "Mounted Achromatic Doublets, AR Coated: 400 - 700 nm," Thorlabs, [Online]. Available: https://www.thorlabs.com/newgrouppage9.cfm?objectgroup_id=2696. [Accessed 25 July 2016].

[22] "CP-3800 GC Getting Started Manual," Varian, Inc, Walnut Creek, CA, 1999.

[23] "CP-3800 GC Operator's Manual," Varian, Inc, Walnut Creek, CA, 2004.

[24] S. R. Turns, An Introduction to Combustion Concepts and Application, University Park,PA: Mc Graw Hill, 2012.